Cell Reports

Article

The composition of the gut microbiota following early-life antibiotic exposure affects host health and longevity in later life

Graphical abstract

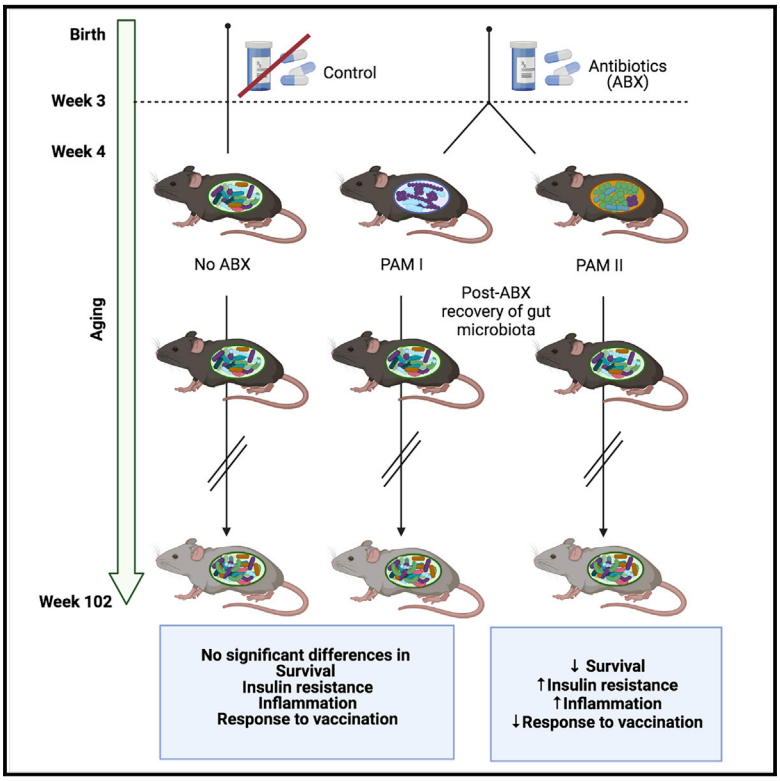

Highlights

- Analysis of aged mice exposed to antibiotics in the pre-weaning period
- Microbiota community type following antibiotics affects host health in later life
- PAM II mice have increased insulin resistance, inflammaging, and reduced lifespan

Authors

Miriam A. Lynn, Georgina Eden, Feargal J. Ryan, ..., Steve L. Wesselingh, Geraint B. Rogers, David J. Lynn

Correspondence

david.lynn@sahmri.com

In brief

Lynn et al. expose mice to antibiotics in early life and then monitor these mice for more than 700 days. The study reveals that differences in the composition of the gut microbiota following antibiotic exposure differentially affects host immunity, metabolism, and longevity in later life.

Lynn et al., 2021, Cell Reports *36*, 109564
August 24, 2021
https://doi.org/10.1016/j.celrep.2021.109564

CellPress

Cell Reports

CellPress
OPEN ACCESS

Article

The composition of the gut microbiota following early-life antibiotic exposure affects host health and longevity in later life

Miriam A. Lynn,[1,7] Georgina Eden,[1,7] Feargal J. Ryan,[1] Julien Bensalem,[2] Xuemin Wang,[3,4] Stephen J. Blake,[1] Jocelyn M. Choo,[1,5] Yee Tee Chern,[1] Anastasia Sribnaia,[1] Jane James,[1] Saoirse C. Benson,[1,5] Lauren Sandeman,[3] Jianling Xie,[3] Sofia Hassiotis,[2] Emily W. Sun,[5] Alyce M. Martin,[5] Marianne D. Keller,[6] Damien J. Keating,[5] Timothy J. Sargeant,[2] Christopher G. Proud,[3,4] Steve L. Wesselingh,[1,5] Geraint B. Rogers,[1,5] and David J. Lynn[1,5,8,*]

[1]Precision Medicine Theme, South Australian Health and Medical Research Institute, Adelaide, SA 5001, Australia
[2]Hopwood Centre for Neurobiology, Lifelong Health Theme, South Australian Health and Medical Research Institute, Adelaide, SA 5001, Australia
[3]Lifelong Health Theme, South Australian Health & Medical Research Institute, Adelaide, SA 5000, Australia
[4]School of Biological Sciences, University of Adelaide, Adelaide, SA 5005, Australia
[5]Flinders Health and Medical Research Institute, Flinders University, Bedford Park, SA 5042, Australia
[6]Preclinical, Imaging & Research Laboratories (PIRL), South Australian Health & Medical Research Institute, Adelaide, SA 5000, Australia
[7]These authors contributed equally
[8]Lead contact
*Correspondence: david.lynn@sahmri.com
https://doi.org/10.1016/j.celrep.2021.109564

SUMMARY

Studies investigating whether there is a causative link between the gut microbiota and lifespan have largely been restricted to invertebrates or to mice with a reduced lifespan because of a genetic deficiency. We investigate the effect of early-life antibiotic exposure on otherwise healthy, normal chow-fed, wild-type mice, monitoring these mice for more than 700 days in comparison with untreated control mice. We demonstrate the emergence of two different low-diversity community types, post-antibiotic microbiota (PAM) I and PAM II, following antibiotic exposure. PAM II but not PAM I mice have impaired immunity, increased insulin resistance, and evidence of increased inflammaging in later life as well as a reduced lifespan. Our data suggest that differences in the composition of the gut microbiota following antibiotic exposure differentially affect host health and longevity in later life.

INTRODUCTION

The intestinal microbiota consists of a diverse ecosystem of microbes that have been increasingly established to play a wide range of roles in supporting homeostasis, metabolism, and immunity not only in the gut but throughout the body. Disruption of the normal balance of the gut microbiota (for example, via antibiotic exposure) has been associated with a range of metabolic and immune-mediated diseases, including obesity, metabolic disease, type I diabetes, autoimmune disease, and allergic asthma (Cox and Blaser, 2015). The effects appear to be particularly acute in early life (Knoop et al., 2017; Al Nabhani et al., 2019; Cho et al., 2012). A number of studies have shown, for example, that administering antibiotics to mice in early life induces significant increases in total and fat mass (Cox et al., 2014; Nobel et al., 2015). Increasing evidence also suggests that the composition of the gut microbiota is associated with overall lifespan. For example, increased gut microbiota diversity as well as the relative abundance of specific taxa (such as members of *Blautia*, Clostridia, and Lachnospiraceae), have been found to be highly predictive of longevity in Chinese and Italian populations (Kong et al., 2016; Biagi et al., 2016). The composition of the gut microbiota has also been shown to be predictive of age (Galkin et al., 2020; Rothschild et al., 2020) and mortality (Salosensaari et al., 2020). However, proving that the gut microbiota plays a causative role in aging and/or longevity is challenging. Furthermore, it is difficult to determine whether any association between the gut microbiota and lifespan is primarily due to effects in early life or effects due to the well-documented changes in the composition and diversity of the gut microbiota during aging (Maynard and Weinkove, 2018).

To date, studies investigating links between the gut microbiota and longevity have largely been restricted to invertebrate model organisms (Clark and Walker, 2018). Treating *E. coli*, a food source in the lab for *Caenorhabditis elegans*, with UV light, heat, or antibiotics has, for example, been shown to extend the lifespan of *C. elegans* (Garigan et al., 2002). Furthermore, targeting specific metabolic pathways in *E. coli*, such as folate synthesis, can extend the *C. elegans* lifespan without altering bacterial growth (Virk et al., 2012), and a screen of nearly 4,000 *E. coli* gene deletions identified 27 gene mutants that extended the *C. elegans* lifespan (Han et al., 2017). In *Drosophila*, age-related

increases in Gammaproteobacteria have been shown to precede compromised gut barrier integrity, increased levels of proinflammatory cytokines, and shortened lifespan (Clark et al., 2015). Expression of the *Drosophila* intestinal junction protein Snakeskin limits gut microbial dysbiosis and promotes increased longevity (Salazar et al., 2018). In contrast, transient exposure of *Drosophila* to low concentrations of oxidants in early life has also been shown to extend the lifespan in a manner that is dependent on the oxidants acting in an antibiotic-like manner (Obata et al., 2018). These data suggest that effects on the gut microbiota in early and later life may affect the lifespan.

Few studies have investigated a causative relationship between the gut microbiota and longevity in vertebrates. A study in the African turquoise killifish, however, supports the case that the gut microbiota is an important factor in regulating vertebrate lifespan (Smith et al., 2017). Recolonizing the gut of middle-aged killifish with bacteria from young donor killifish prevented the decrease in microbial diversity associated with host aging and led to an extended lifespan. In mice, age-associated intestinal dysfunction and inflammation have been found to be decreased significantly in germ-free mice (Thevaranjan et al., 2017), and a higher proportion of germ-free mice have been observed to live to 600 days compared with their conventional counterparts. Moreover, colonizing young germ-free mice with the microbiota of old conventionally colonized mice led to significantly increased gut permeability and inflammation (Thevaranjan et al., 2017). However, this was not observed in similar studies by other researchers (Kundu et al., 2019), suggesting that the composition of the donor microbiota is important. Mice treated with the α-glucosidase inhibitor acarbose, which is known to increase the median lifespan, display a correlation between microbiota-produced short-chain fatty acids (SCFAs) and lifespan (Smith et al., 2019). Furthermore, two recent studies in genetically deficient mice with a significantly impaired lifespan (progeroid mice and regulatory T cell-deficient scurfy mice) found that modifying the gut microbiota could extend the lifespan (Bárcena et al., 2019; He et al., 2019).

Although these studies strongly suggest that the microbiota plays an important role in regulating lifespan, to our knowledge, no study to date has investigated whether early-life antibiotic-driven disruption of the gut microbiota impairs the lifespan in otherwise healthy, normal chow-fed, wild-type mice. Here we report that administering antibiotics to mice in the preweaning period led to a reduced lifespan in later life in a manner that appears to be dependent on the composition of the low-diversity microbiota that recolonizes the gut following antibiotic exposure. The group of antibiotic-exposed mice with a reduced lifespan (post-antibiotic microbiota [PAM] II mice) also had impaired immunity, increased insulin resistance, and increased interleukin-1β (IL-1β) levels in serum, suggesting that increased inflammaging and metabolic dysfunction are important factors leading to a reduced lifespan in these mice.

RESULTS

Different low-diversity microbiota community types colonize the gut following antibiotic exposure

To investigate whether dysregulation of the gut microbiota following antibiotic exposure in early life is associated with a decreased lifespan, we used an established mouse model of early-life antibiotic exposure (Lynn et al., 2018) where dams and their pups (n = 20) were exposed to ampicillin and neomycin via their drinking water in late pregnancy (from embryonic day 14) and throughout the preweaning mouse infant period (until ~day 21 after birth). At weaning, littermate antibiotic-exposed pups were randomized to different cages. The mice were then maintained alongside a control group of pups (n = 20) that were not exposed to antibiotics under the same housing conditions for the duration of the experiment. Both groups of mice were fed a normal chow diet. We profiled the composition of the fecal microbiota of these mice throughout their lifespan by 16S rRNA gene sequencing (Figures 1A and 1B). 16S rRNA gene sequencing revealed that, in comparison with unexposed (No ABX) mice, antibiotic exposure (ABX) resulted in significant changes to the composition of the gut microbiota 1 week after exposure (week 4 of life) (Figures 1C–1H). Antibiotic-exposed mice were recolonized by two distinct microbiota community types (Figures 1C–1F). We refer to these mice as PAM I (n = 10) and PAM II (n = 10). PAM I mice (2 cages, n = 5/cage) were recolonized predominantly by Erysipelotrichaceae (*Turicibacter*) and Enterococcaceae (Figure 1D). In contrast, PAM II mice (2 cages, n = 5/cage) were recolonized predominantly by members of the Lachnospiraceae, including *Blautia* and *Coprococcus* (Figure 1E). The composition of the microbiota in one PAM I mouse was more similar to PAM II mice (with a high relative abundance of *Blautia*), which we confirmed by qPCR (data not shown), demonstrating that, even within cages, significant variation in the composition of the microbiota following antibiotics can occur. PAM I and PAM II mice had significantly decreased Chao1 indices at week 4 of life compared with No ABX mice, indicating significantly decreased species richness (Figure 1G). Other metrics, such as Faith's phylogenetic diversity and Shannon's diversity, also revealed a significant loss of diversity in PAM I and PAM II mice (data not shown). Next we used PICRUSt2 (Douglas et al., 2020) to predict the metagenomic functions of the microbiota in each group, which suggested that the microbiota in PAM I and PAM II mice had substantially different functional capacity (Figure 1H). The relative abundance of more than 200 MetaCyc pathways was predicted to be significantly different among the 3 groups of mice (FDR < 0.05; Table S1). These pathways included a range of bacterial metabolic pathways, including several involved in SCFA fermentation (Figures S1A–S1E). The effects of antibiotic exposure we observed, including a significant loss of diversity, blooms of enterobacteria and other pathobionts, and inter-individual/cage variation in the response of the gut microbiota to antibiotics, are consistent with the effects reported previously by us and others in mice (Lynn et al., 2018; Ng et al., 2019) and humans (Bokulich et al., 2016; McDonnell et al., 2021; Dethlefsen and Relman, 2011; Hildebrand et al., 2019; Palleja et al., 2018). We hypothesized that different low-diversity microbiota community types that colonize the gut following antibiotic exposure would differentially affect immunity and metabolism in later life, potentially influencing overall lifespan. To investigate this, we defined PAM I and PAM II mice as two separate experimental groups for the rest of the experiment. The 3 groups of mice (No ABX, PAM I, and PAM II) were therefore defined *a priori*, before any data were collected on lifespan, metabolism, or immunity in later life.

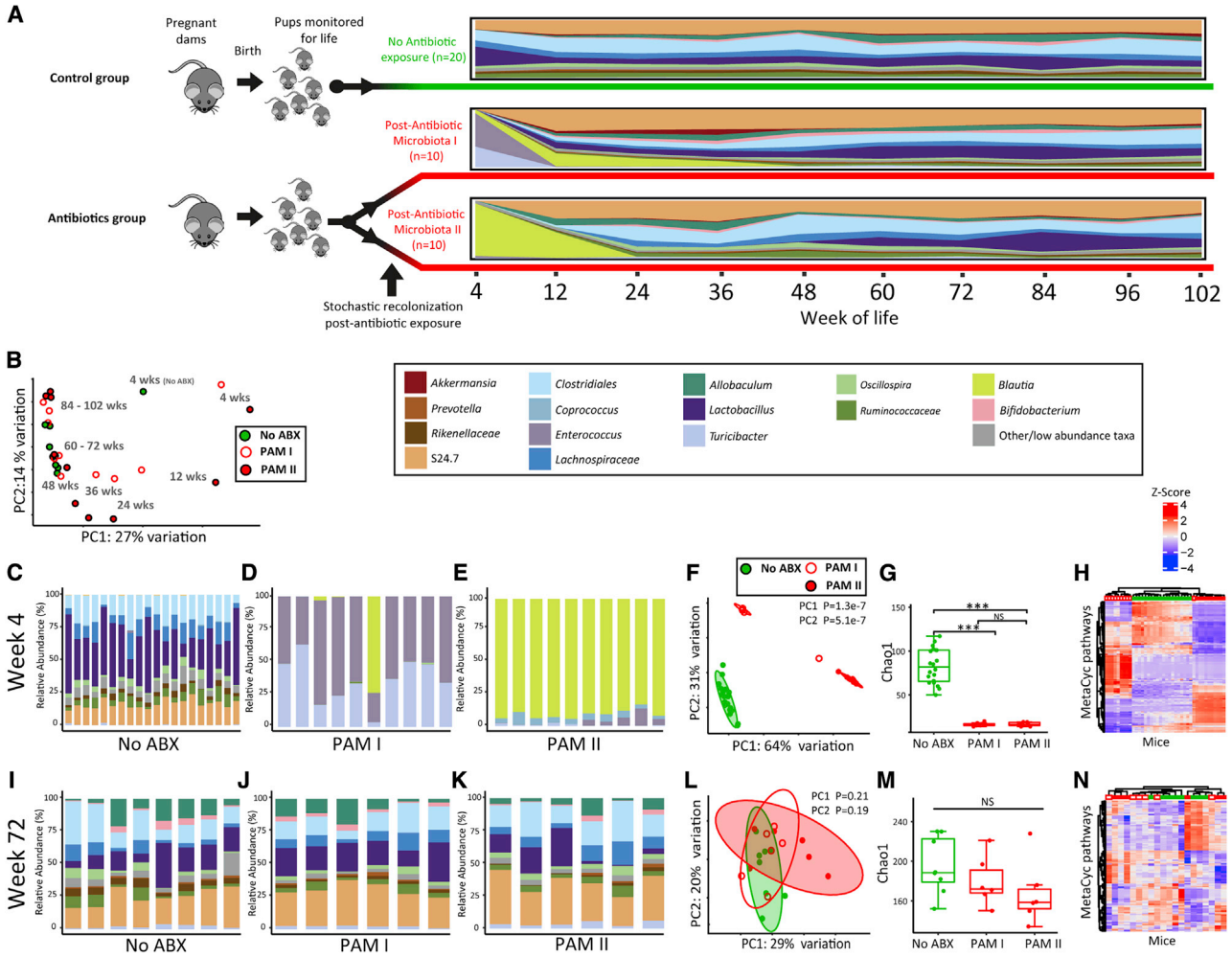

Figure 1. Study design and composition of the fecal microbiota in antibiotic-exposed and unexposed mice throughout life

(A) The composition of microbiota in unexposed mice (No ABX, n = 20) and mice exposed to antibiotics in early life (n = 20) was profiled using 16S rRNA gene sequencing of DNA extracted from pooled fecal samples collected at specific intervals from 1 week after antibiotic exposure (week 4 of age) to week 102 of life. Two distinct microbiota were evident after antibiotic exposure (PAM I and PAM II, n = 10/group).

(B) Principal-component analysis (PCA) of Bray-Curtis dissimilarity indices.

(C–N) Composition, diversity, and predicted metagenome functional capacity of the fecal microbiota at weeks 4 and 72 of life. Each barplot represents the relative abundance of major taxa in samples collected from individual mice at week 4 (C–E) and week 72 of life (I–K). PCA plots are based on Bray-Curtis dissimilarities (F and L). A Kruskal-Wallis test was used to assess differences in the PC1 and PC2 values between groups. Data in (G) and (M) are represented as box and whisker plots. Statistical significance in (G) and (M) was assessed using a Wilcoxon rank-sum test (NS, not significant; ***$p < 0.001$).

(H and N) Heatmaps of PICRUSt2-inferred metagenome functions. Intensity represents the *Z* score normalized predicted relative abundance of MetaCyc pathways.

The effect of antibiotic exposure on the composition of the microbiota was evident until approximately 36–48 weeks of age (Figures 1A and 1B). We have previously reported the effects of antibiotic exposure on the murine gut microbiota to persist to at least 13 weeks of age (Lynn et al., 2018), and antibiotic exposure has been shown to perturb the human gut microbiota for up to 1–4 years following exposure, depending on the antibiotic prescribed (Ainonen et al., 2021; Jernberg et al., 2007; Mulder et al., 2020). For example, in a study of the gut microbiota of 1,413 adults following antibiotic exposure, alpha diversity was found to be significantly lower and community type altered significantly for up to 4 years after prescription of macrolides or lincosamides (Mulder et al., 2020). By 72 weeks of age (Figures 1I–1N), there were no significant differences in beta diversity (Figure 1L) or Chao1 richness (Figure 1M) detectable between any of the 3 groups of mice, nor was the relative abundance of any individual genus or predicted MetaCyc pathway significantly different between groups at this time (Figure 1N). We also performed further 16S rRNA gene sequencing of samples collected at weeks 84, 96, and 102 (Figures S1F–S1W). Although some relatively minor differences were detected at week 96 (Figures S1L–S1Q), no differences were evident at 84 or 102 weeks, and it appeared that the fecal microbiota across the 3 experimental groups was highly similar later in life (Figure S1). These

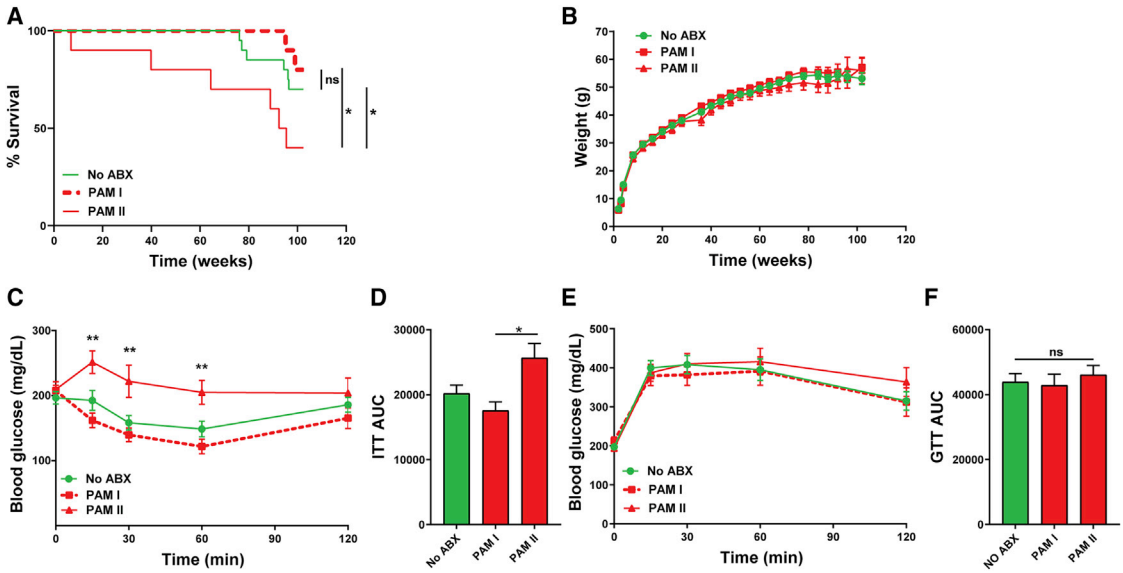

Figure 2. Early-life antibiotic exposure leads to a significantly reduced lifespan and increased insulin resistance in PAM II mice

(A) PAM II mice had significantly poorer survival compared with untreated or PAM I mice. No ABX (n = 20), PAM I (n = 10), PAM II (n = 10). Statistical significance was assessed using a Breslow-Wilcoxon test.

(B) There were no significant differences in the body weights of unexposed (No ABX) and antibiotic-exposed PAM I and PAM II mice. A mixed-effects model implemented in Prism was used to assess statistical significance.

(C) An i.p. insulin tolerance test (ITT) conducted at week 94 of life.

(D) Area under the curve of the data in (C).

(E) An i.p. glucose tolerance test (GTT) in mice at week 95 of life.

(F) Area under the curve of the data in (E).

Data in (B)–(F) are represented as the mean ± SEM. Statistical significance was assessed using a two-way (C and E) or one-way ANOVA (D and F) with Tukey's correction for multiple comparisons. *$p < 0.05$, **$p < 0.01$.

data suggested that any phenotypic differences identified in later life were more likely driven by antibiotic-driven differences in the composition and function of the microbiota in early life.

PAM II mice developed increased insulin resistance and inflammaging in later life and had a significantly shortened lifespan

To determine whether colonization by different community types following antibiotic exposure was associated with a reduced lifespan, we monitored the survival of PAM I, PAM II, and No ABX mice until ~102 weeks of age. At this time point, any remaining mice were culled humanely to collect tissue, including intestine, liver, muscle, and brain, for further analysis. Interestingly, we observed that PAM II mice had a significantly decreased lifespan ($p < 0.05$) compared with No ABX mice or PAM I mice (Figure 2A). In the assessment period, 6 of 10 mice were found dead or reached humane endpoints in the PAM II group compared with half as many (6 of 20) in the untreated control group and only 2 of 10 in the PAM I group (Table S2). Where possible (i.e., when the carcass was discovered quickly enough to enable assessment), the carcass of each deceased mouse was assessed by the institute's veterinary officer for any gross pathologies that could suggest a cause of death. A consistent cause of death was not evident, but liver damage and palpable masses were noted in several deceased PAM II mice (Pettan-Brewer and Treuting, 2011). Necroscopy revealed that mice in all groups also had enlarged seminal vesicles (data not shown), as reported previously in aged mice (Finch and Girgis, 1974; Pettan-Brewer and Treuting, 2011). Unlike prior studies that have shown a link between early-life antibiotics and obesity (Cox and Blaser, 2015), we did not detect any significant differences in the body weights of either group of PAM mice compared with No ABX mice or between PAM I and PAM II mice (Figure 2B). Body fat composition, assessed at 96 weeks of age, was also not significantly different (Figure S2A).

Although there were no obvious signs of metabolic dysfunction (i.e., weight gain) in the antibiotic-exposed mice, we assessed glucose homeostasis under physiological stress by performing intraperitoneal (i.p.) insulin resistance and glucose tolerance tests at ~95 weeks of age in the 3 groups of mice. PAM II mice (poorer survival group) had significantly increased insulin resistance compared with PAM I or No ABX mice (Figures 2C and 2D) despite no differences in baseline serum insulin levels (Figure S2B). In contrast, glucose tolerance was not significantly different between any of the groups (Figures 2E and 2F), although, as reported previously, baseline glucose levels in all 3 groups of aged mice were notably higher than levels normally observed in younger mice (Reynolds et al., 2019). Peripheral serotonin (5-hydroxytryptophan [5-HT]) levels, which have been shown recently to regulate host glucose homeostasis in a manner that is mediated by the gut microbiota (Martin et al., 2019), were also not significantly different between the 3 groups

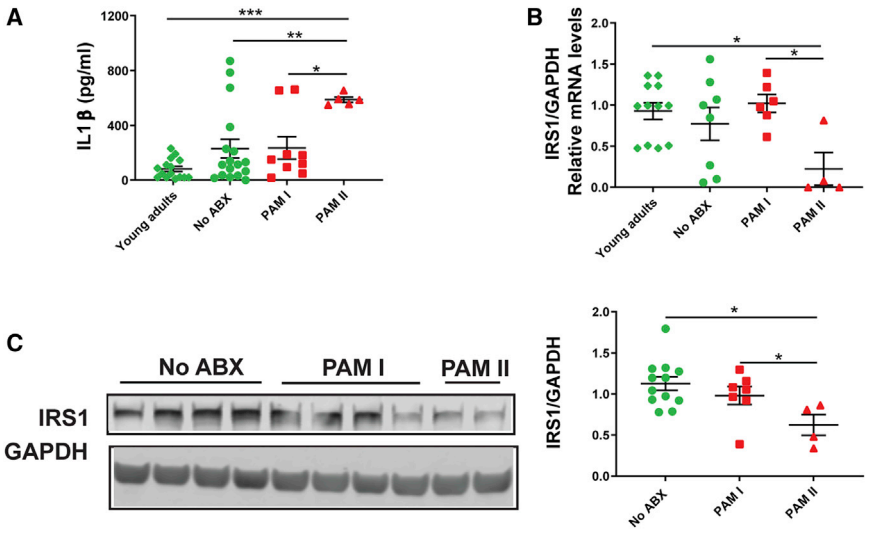

Figure 3. PAM II mice had significantly increased IL-1β cytokine levels in serum

(A) Levels of IL-1β in the serum of mice at 92 weeks of age were assessed by ELISA.

(B and C) IRS1 mRNA (B) and protein levels (C) were assessed in gastrocnemius muscle by qPCR or western blotting. Muscle tissue was collected from No ABX, PAM I, and PAM II mice at 102 weeks of age. A representative of two different western blots is shown.

Data are represented as the mean ± SEM. Statistical significance was assessed using a one-way ANOVA with Tukey's correction for multiple comparisons. *p < 0.05, **p < 0.01, ***p < 0.001.

(Figure S2C), although 5-HT levels were elevated significantly in all aged mice compared with young adult controls, as reported previously (data not shown) (Nahata et al., 2013). There were also no significant differences in glucagon levels (Figure S2D) or in the homeostatic model assessment of β-cell function (HOMA-β) or HOMA of insulin resistance (HOMA-IR) indices (Figures S2E and S2F).

Because increased inflammatory responses in later life are a characteristic of metabolic syndrome (Economopoulos et al., 2016) and inflammaging (Frasca and Blomberg, 2016), we assessed the levels of the inflammatory cytokines IL-1β, interferon γ (IFNγ) and tumor necrosis factor alpha (TNF-α) in serum collected at 60, 84, and 92 weeks in comparison with young adult controls. IL-1β levels were increased significantly in PAM II mice at 92 weeks compared with No ABX and PAM I mice (Figure 3A). IL-1β levels were not increased significantly in PAM II mice at 60 and 84 weeks (Figure S2G). There was no significant difference in IFNγ or TNF-α levels between the 3 groups of mice at any time points (Figures S2H and S2I), although IFNγ levels in PAM I mice at 92 weeks of age were significantly higher than in young adult controls. IL-1β has been shown to have a pathogenic role in development of insulin resistance (Bing, 2015; Jager et al., 2007). The significantly increased levels of IL-1β in PAM II mice are consistent with the greater insulin resistance we observed in PAM II mice (Figure 2C). IL-1β has been shown to inhibit insulin signaling by reducing tyrosine phosphorylation of insulin receptor substrate 1 (IRS1) and decreasing IRS1 expression (Aye et al., 2013; Copps and White, 2012). IRS1 plays a critical role in signaling downstream of the insulin receptor. Because muscle is quantitatively the most important tissue for insulin-stimulated glucose uptake, we assessed levels of IRS1 in the gastrocnemius muscle of No ABX, PAM I, and PAM II in comparison with young adult control mice. Consistent with the increased levels of IL-1β and the increased insulin resistance observed in PAM II mice, IRS1 mRNA and protein expression was decreased significantly in the gastrocnemius muscle of PAM II mice (Figures 3B and 3C). These data suggest that elevated levels of IL-1β in PAM II mice in later life exacerbate age-related insulin resistance via decreased IRS1 levels. Importantly, these effects appear to be dependent on the composition of the microbiota that recolonizes the gut following antibiotic exposure because they were only observed in PAM II mice.

PAM II mice had significantly increased microglia staining in the dentate gyrus region of the brain

To investigate whether differences in inflammaging were evident in other tissues, we collected brain, spleen, and liver from mice in each of the 3 groups that were still alive at 102 weeks of age and from young adult control mice. The severity of steatosis (Liang et al., 2014) and inflammation (Mayer et al., 2014) in the liver was scored across specimens in a blinded fashion as described in the STAR Methods. Histopathological scoring of the liver did not reveal any significant differences between the 3 groups of mice (Figure S3A), although all aged mice had significantly higher histopathology scores compared with young adult control mice, indicating increased liver inflammation in the aged mice. We also assessed levels of lipocalin-2, an established marker of gut inflammation, in fecal samples collected at week 88. Consistent with the fact that the composition of the gut microbiota was comparable between the 3 groups in later life, no significant differences in lipocalin-2 levels were evident (Figure S3B).

As the brain ages, cognitive function decreases, with hippocampal function particularly badly affected with age (O'Shea et al., 2016). Furthermore, previous studies have revealed that the microbiota regulates the maturation and function of microglia in the brain (Erny et al., 2015). Given these data, we next quantified total microglia in the dentate gyrus of the hippocampus using immunostaining for ionized calcium binding adaptor molecule 1 (IBA1). IBA1$^+$ microglia were increased significantly in the dentate gyrus of PAM II mice (Figure S3C), consistent with the increased inflammaging observed in these mice in other tissues. Increased numbers of IBA1$^+$ microglia have also been reported previously in germ-free mice (Erny et al., 2015). Another study has also reported that germ-free mice receiving a microbiota transplant from old mice had more doublecortin-positive (DCX$^+$) neurons in the dentate gyrus, surprisingly indicating increased neurogenesis, than germ-free mice receiving a microbiota transplant from young mice (Scott et al., 2020). Given this,

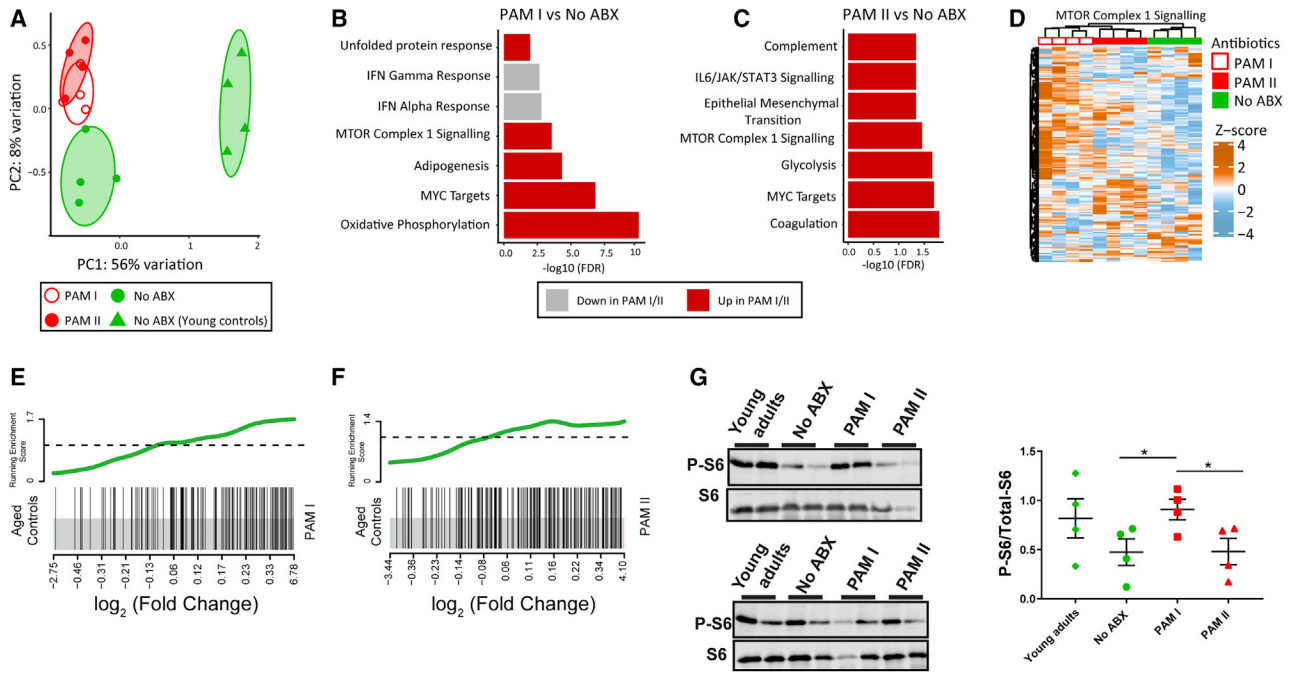

Figure 4. Gene expression in the livers of 102-week-old (No ABX, PAM I, and PAM II) mice and young adult control mice was profiled using RNA-seq

(A) Multidimensional scaling (MDS) analysis of the gene expression data.

(B and C) Gene Set Enrichment Analysis (GSEA) of liver gene expression in PAM I or PAM II mice compared with No ABX controls. See also Table S3.

(D) Heatmap of gene expression in the MSigDB-annotated mTOR complex 1 signaling pathway. Intensity represents the *Z* scores of $\log_2$ read counts per million. Genes are shown on the y axis and samples on the x axis.

(E and F) Barcode plots representing the enrichment of mTOR complex 1 signaling in PAM I (E) and PAM II (F) mice relative to No ABX controls.

(G) Levels of phosphorylated S6 (P-S6) were assessed by western blotting (two separate blots are shown) relative to total S6. n = 4/group.

Data are represented as the mean ± SEM. A two tailed t test was used to assess statistical significance in (G). *p < 0.05.

we also assessed the number of DCX^+ neurons in young, aged No ABX, PAM I, and PAM II mice. Although clearly evident in young mice, DCX^+ neurons were almost completely absent in all 3 groups of aged mice (Figure S3D).

PAM II mice had significantly decreased influenza-specific antibody responses

Next we assessed whether there were differences in any immune cell populations that could explain the increased inflammaging observed in PAM II mice. Flow cytometry analysis was used to assess immune populations in the spleen, including T cells (memory, naive, $PD1^+$, and regulatory T [Treg] cells), B cells, natural killer (NK) cells, macrophage/monocytes, neutrophils, and conventional DCs (cDCs). Consistent with previous reports (Chen et al., 2013; Beli et al., 2014), NK cells, cDCs and naive $CD8^+$ and $CD4^+$ T cells were decreased significantly in aged mice compared with young adult controls (Figures S4A–S4D), whereas memory T cells, $PD1^+$ T cells, and $FoxP3^+$ regulatory T cells (Tregs) were increased significantly (Figures S4E–S4I). There was no significant difference in B cells between young and aged mice (Figure S4J). None of the immune cell populations assessed were significantly different between aged No ABX, PAM I, or PAM II mice. We also assessed antibody responses to the influenza vaccine (administered to aged mice at 84 weeks) and found that PAM II mice had significantly lower influenza-specific immunoglobulin G $(IgG)_{Total}$ responses to vaccination compared with PAM I mice (Figure S4K). There were no significant differences in (non-antigen specific) total IgG (Figure S4L), indicating that it was the response to vaccination that was impaired as opposed to a gross defect in humoral immunity. As reported previously (McDonald et al., 2017; Baldwin et al., 2018), aged mice in all three groups (No ABX, PAM I, and PAM II) had significantly impaired IgG_{Total} antigen-specific antibody responses to the influenza vaccine in comparison with young adult mice (Figure S4K).

RNA sequencing reveals dysregulation of liver metabolism and immune function in PAM I and PAM II mice

To further characterize changes in metabolism and immunity in PAM I and PAM II mice, we used RNA sequencing (RNA-seq) to profile transcriptome-wide gene expression in the liver of PAM I and PAM II mice in comparison with No ABX aged mice and young adult control mice (n = 4/group; ~60 million reads/sample). Multidimensional scaling (MDS) analysis revealed that the largest source of variation in gene expression was, as expected, between aged and young mice (Figure 4A). Gene set enrichment analysis (GSEA) and pathway over-representation

analysis identified a broad range of pathways related to inflammation and fatty acid metabolism (Figures S5A–S5C) that were upregulated in the livers of aged No ABX mice compared with young adult controls. These data were consistent with previous studies that assessed gene expression in the livers of aged mice (White et al., 2015) and rats (Shavlakadze et al., 2019). Importantly, GSEA also revealed that the expression of genes in a range of pathways and processes associated with metabolism and the immune response were altered in PAM I and PAM II mice compared with No ABX mice (Figures 4B and 4C). Many of these pathways have been linked to an altered lifespan in previous studies, including MYC proto-oncogene, bHLH transcription factor (MYC) signaling (Hofmann et al., 2015), oxidative phosphorylation (Brace et al., 2016), and the unfolded protein response (Labunskyy et al., 2014). Of particular interest was the upregulation of genes involved in the mammalian target of rapamycin complex 1 signaling (mTORC1) pathway in PAM I and PAM II mice (Figures 4D–4F), which has been strongly implicated in regulating lifespan (Harrison et al., 2009). To further investigate mTORC1 signaling in these mice, we assessed the levels of phosphorylated S6 ribosomal protein (P-S6) in the liver relative to total S6. P-S6/S6 is a well-established functional readout of mTORC1 activity (Hay and Sonenberg, 2004). Consistent with the stronger upregulation of mTORC1 signaling pathway at a gene expression level in the livers of PAM I mice, P-S6 was increased significantly in the liver of these mice compared with aged No ABX and PAM II mice but not young mice (Figure 4G).

Colonization of germ-free mice with the PAM I or PAM II microbiota alters immune responses in early life

Al Nabhani et al. (2019) have reported that, at weaning, the intestinal microbiota induces a strong immune response peaking around day 21 of age, which they term a "weaning reaction." This weaning reaction is programmed in time and when inhibited can lead to a pathological imprinting that drives disease susceptibility in later life. In our study, recolonization of the gut microbiota following antibiotic exposure coincided with the timing of this reaction. A plausible scenario is therefore that colonization with the PAM I or PAM II microbiota following antibiotic exposure modulated this weaning reaction in different ways, reprogramming immune development trajectories in PAM I and PAM II mice. To investigate this, we colonized 14-day-old germ-free (GF) mice with the PAM I or PAM II microbiota using fecal microbiota transplantation (FMT) and assessed markers of the weaning reaction and other immune responses on day 21 of life compared with GF and specific-pathogen-free (SPF) mice (Figure 5A). 16S rRNA gene sequencing of fecal samples collected from the original PAM I and PAM II mice as well as GF+PAM I and GF+PAM II mice confirmed faithful transfer of the PAM I and PAM II microbiota to recipient mice (Figures 5B and 5C).

Consistent with the data from Al Nabhani et al. (2019), we observed a similar weaning reaction in normally colonized SPF mice on day 21 of age that was lacking in GF mice. This response was characterized by significantly enhanced expression of *Ifng* and *Tnfa* in the ileum of SPF mice compared with GF mice (Figure 5D) and by significantly increased numbers of IFNγ^+ CD45$^+$ lymphocytes, IFNγ^+ CD3$^+$ T cells, and IFNγ^+ CD8$^+$ T cells in the *lamina propria* of the small intestine of SPF mice compared with GF mice (Figure 5E). Interestingly, GF+PAM II but not GF+PAM I mice had significantly increased *Ifng* expression in the ileum on day 21 of age compared with GF mice (Figure 5Di). In contrast, GF+PAM I but not GF+PAM II mice had significantly increased *Tnfa* expression in the ileum on day 21 of age compared with GF mice (Figure 5Dii). Additionally, in comparison with GF mice, colonization with the PAM II but not PAM I microbiota was sufficient to induce significantly increased numbers of IFNγ^+CD45$^+$ lymphocytes and IFNγ^+CD8$^+$ T cells in the *lamina propria* of the small intestine (Figure 5E).

We also assessed whether colonization with the PAM I or PAM II microbiota was associated with any other differences in immune responses in the peripheral blood or spleen. Levels of TNF-α in blood collected from GF+PAM II mice were significantly higher compared with GF+PAM I, GF, and SPF mice (Figure 5Fi), suggesting increased inflammation in GF+PAM II mice. Next we stimulated blood collected from the four groups of mice with lipopolysaccharide (LPS) and found that TNF-α levels were increased significantly following stimulation of blood from GF and GF+PAM I mice, although responses were muted compared with LPS-stimulated blood collected from SPF mice (Figure 5Fii). In contrast, blood collected from GF+PAM II mice was unresponsive to LPS stimulation, suggesting endotoxin tolerance in GF+PAM II mice. Interestingly, splenocytes from GF+PAM I and GF+PAM II mice stimulated with LPS had responses comparable with SPF mice (Figure 5G). These data suggest that colonization with the PAM I or PAM II microbiota differentially affects a previously described weaning reaction in the intestine that has been shown to imprint on immune development in later life and also alters immune responses in the peripheral blood. These data provide a plausible explanation for the differences in immunity, metabolism, and lifespan we observed in PAM I and PAM II mice in later life, but further work is now required to demonstrate causal links by following GF+PAM I/II mice for the duration of their lives.

DISCUSSION

A growing number of studies have reported associations between the composition of the gut microbiota with healthspan and lifespan in human populations (Claesson et al., 2012; Biagi et al., 2016); however, whether these associations reflect a causative relationship or simply reflect differences in diet, genetics, or environment in individuals with increased longevity remains to be proven. Studies in short-lived invertebrate models, such as *Drosophila* (Clark et al., 2015) or *C. elegans* (Han et al., 2017), are, however, highly supportive of a causative relationship. These studies suggest that the gut microbiota may significantly influence health/lifespan by modulating systemic chronic immune activation, known as "inflammaging" (Biagi et al., 2016), and by contributing to tumorigenesis (Biragyn and Ferrucci, 2018). Recent studies in mice that have a significantly reduced lifespan because of a genetic deficiency (progeroid mice and Treg cell-deficient scurfy mice), have also supported a link between the gut microbiota and mammalian lifespan (He et al., 2019). Whether the links between the gut microbiota and healthy aging (and, ultimately, longevity) are driven primarily by age-related changes in the gut microbiota or are also influenced by

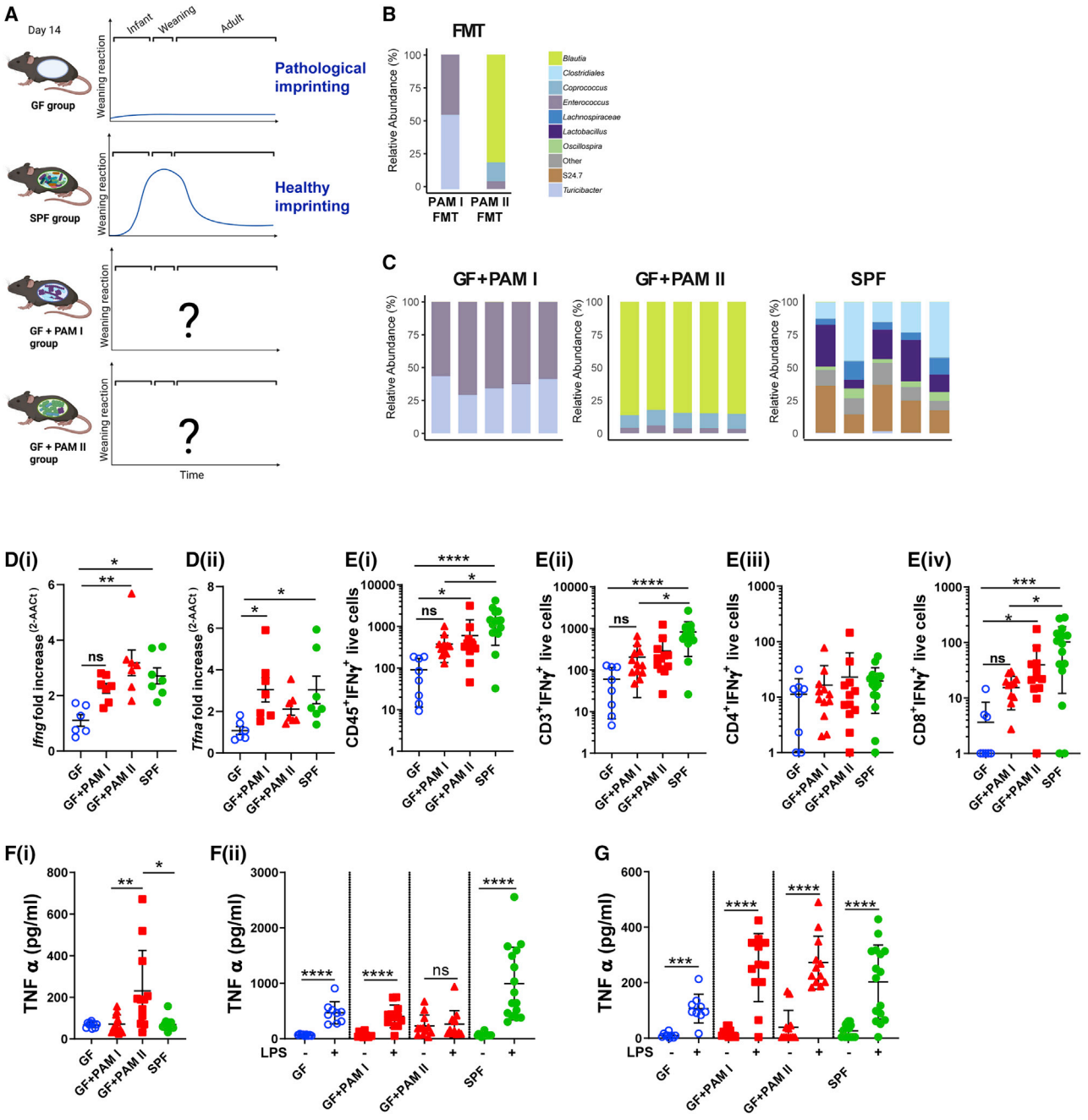

Figure 5. Colonization of germ-free (GF) mice with the PAM I or PAM II microbiota differentially affects immune responses in early life

(A) GF pups were maintained as GF or were colonized with the PAM I and PAM II microbiota at day 14 of life.

(B and C) The composition of (B) the PAM I and PAM II fecal microbiota transplantation (FMT) material prior to FMT and (C) the cecal contents of the GF+PAM I and GF+PAM II mice were profiled using 16S rRNA gene sequencing.

(D) *Ifng* and *Tnfa* gene expression in the ileum of GF, GF+PAM I, GF+PAM II, and SPF mice was determined by qRT-PCR.

(E) The number of IFNγ^+ lymphoid cells in small intestine *lamina propria* of GF, GF+PAM I, GF+PAM II, and SPF mice. CD45$^+$ cells were gated on live cells, CD3$^+$ T cells were gated on CD45$^+$ cells, and CD4$^+$ and CD8$^+$ T cells were gated on CD3$^+$CD45$^+$ cells.

(F and G) Blood (F) and splenocytes (G) were collected from GF, GF+PAM I, GF+ PAM II, and SPF mice at day 21 of age, erythrocyte depleted, and stimulated with LPS (10 ng/mL) for 18 h. TNF-α production in the supernatant was assessed via ELISA.

Data are represented as the mean ± SEM. Statistical significance in (D), (E) and (F(i)) was assessed using a Kruskal-Wallis test with Tukey's correction for multiple comparisons. Pairwise statistical significance in (F(ii)) and (G) was assessed using a Mann Whitney test. *p < 0.05, **p < 0.01, ***p < 0.001, ****p < 0.0001.

the gut microbiota in early life is currently poorly understood (Biagi et al., 2016; Bárcena et al., 2019; DeJong et al., 2020). Given that the effects of antibiotic-driven disruption of the gut microbiota on immunity and metabolism appear to be particularly acute when exposure occurs in early life (Al Nabhani et al., 2019; Cho et al., 2012), it seems likely that early-life disruption of the microbiota could also influence lifespan.

To investigate whether early-life antibiotic-driven disruption of the gut microbiota influences lifespan in mice, we exposed otherwise healthy, wild-type mice to antibiotics in the pre-weaning period and then monitored these mice in comparison with unexposed control mice for more than 700 days. Antibiotic-exposed mice were colonized by two compositionally and functionally distinct low-diversity microbiota (which we termed PAM I and PAM II mice) despite the fact that these were littermates exposed to the same antibiotics. The effects of antibiotic exposure we observed are consistent with the effects reported previously by us and others in mice (Lynn et al., 2018; Ng et al., 2019) and humans (Bokulich et al., 2016; McDonnell et al., 2021; Dethlefsen and Relman, 2011; Hildebrand et al., 2019; Palleja et al., 2018). The importance of different patterns of recolonization following antibiotic exposure on immunity and metabolism in later life are currently poorly understood.

We found that only PAM II mice had a significantly reduced lifespan. Consistent with the effects on lifespan, these mice also had significantly increased insulin resistance and inflammaging as well as impaired immune responses to vaccination. Our data therefore suggest that the effects of antibiotics in early life on metabolism, immunity, and health in later life could be much more dependent on the composition of the microbiota that recolonizes the gut following antibiotic exposure than appreciated previously. Increasing data suggest that these effects are particularly potent in early life and that there is a "window of opportunity" for the microbiota to systemically influence immunity and metabolism (Cox et al., 2014; Lynn et al., 2018; Al Nabhani et al., 2019). This is reinforced by our observations that the composition, diversity, and predicted metagenomic function of PAM I, PAM II, and control mice converged over time and were not significantly different in later life when differences in metabolism and immunity were evident. These data suggest that differences in the metabolites and/or other immunomodulatory molecules produced by the microbiota in early life lead to long-term reprogramming of metabolism and immunity that manifests in later life with impaired health and longevity. Al Nabhani et al. (2019) have reported that, at weaning, the intestinal microbiota induces a strong immune response, which they term a "weaning reaction." This weaning reaction is programmed in time and when inhibited can lead to pathological imprinting that drives disease susceptibility in later life. We found that colonizing GF mice with the PAM I or PAM II microbiota differentially affected this weaning reaction as well as immune responses in the periphery, providing a plausible explanation for the different effects we observed in PAM I and PAM II mice in later life compared with mice that were not exposed to antibiotics.

Multiple previous studies have reported a link between early-life antibiotic exposure and obesity (Cox and Blaser, 2015; Cox et al., 2014); however, we did not identify any significant differences in body weight or body fat composition in this study. It is important to note that, in our study, mice were fed a normal chow diet for the duration of their lives. Several other studies have also not found a link between early-life antibiotics and body weight (Bäckhed et al., 2007, Cani et al., 2008), even in the presence of a high-fat diet (Murphy et al., 2013). Interestingly, in an independent experiment we conducted with the same experimental design as used in this study (i.e., mice exposed to ampicillin and neomycin in the pre-weaning period), antibiotic-exposed male but not female mice did show significantly increased body weight after 12 months of age (data not shown). Antibiotic-exposed mice in this study were recolonized with a different microbiota than the PAM I and PAM II mice. These data together strongly suggest that the composition and, presumably, the functional capacity of the gut microbiota following antibiotic exposure (rather than its depletion during antibiotics) is a critical factor in driving obesity in later life. These data would also account for the variable associations between antibiotic exposure and obesity reported in different studies.

Antibiotic exposure has a well-established role in modulating glucose metabolism (Livanos et al., 2016). In our study, we observed that PAM II mice had significantly increased insulin resistance and evidence of increased inflammaging, including significantly increased IL-1β in serum and markers suggestive of increased neuroinflammation. These data are consistent with the reduced lifespan observed in PAM II mice. IL-1β has been shown to induce insulin resistance by downregulating IRS1 (Copps and White, 2012; Jager et al., 2007; Aye et al., 2013). Consistent with this, PAM II mice had significantly decreased levels of IRS1 mRNA and protein in muscle tissue. RNA-seq of liver tissue also suggested that mTORC1 signaling was dysregulated in antibiotic-exposed mice (PAM I and, to a lesser extent, PAM II mice). Inhibition of mTORC1 signaling has been strongly implicated in extending the lifespan (Sabatini, 2017); however, if this was the mechanism responsible for the reduced lifespan of PAM II, then we would have expected increased mTORC1 signaling in PAM II mice, whereas P-S6 was higher in the liver of PAM I mice.

Although our study provides several important new insights into the links between the gut microbiota in early life and health and lifespan in later life, it is important to acknowledge several limitations of the study. Conducting our study in otherwise healthy, wild-type, normal chow-fed mice is challenging and costly because each experiment takes more than 2 years to conduct. The long duration of the experiments also makes it very difficult to subsequently test for causal relationships between specific taxa or host/microbial pathways and lifespan. Furthermore, the apparently stochastic nature of recolonization of the gut following antibiotic exposure makes reproducing the same findings very challenging. In fact, as alluded to above, we did attempt this by conducting a second 2-year experiment, but antibiotic exposed mice were recolonized with a different microbiota than the PAM I and PAM II mice in this study and experienced significantly increased body weight but not a reduced lifespan (at least in the period during which we monitored the mice). Future work could expand our initial GF mice experiments to try to tease out the importance of the different taxa that typically dominate the gut microbiota following antibiotic exposure by mono-colonizing GF mice with these taxa and following these mice for their lifespan.

STAR★METHODS

Detailed methods are provided in the online version of this paper and include the following:

- KEY RESOURCES TABLE
- RESOURCE AVAILABILITY
  - Lead contact
  - Materials availability
  - Data and code availability
- EXPERIMENTAL MODEL AND SUBJECT DETAILS
- METHOD DETAILS
  - Antibiotics
  - Germ-free mouse experiments
  - Body composition scanning – EchoMRI
  - Insulin and glucose tolerance test
  - Fecal sampling
  - DNA extraction from fecal samples
  - 16S rRNA gene sequence analysis
  - Vaccination
  - Antibody response
  - Cytokine analysis
  - Measurements of serum glucagon and serotonin
  - RNA extraction
  - RT-qPCR
  - Liver RNA-Seq analysis
  - Splenocyte preparation
  - Immunofluorescent staining for splenocyte flow cytometric analysis
  - Blood and spleen stimulations
  - Protein extraction from muscle and liver
  - Western immunoblotting
  - Liver histology
  - Brain histology and immunohistochemistry
  - Brain image analysis and assessment of immunohistochemistry
  - Lamina propria preparation
  - Immunofluorescent staining for lamina propria cytometric analysis
- QUANTIFICATION AND STATISTICAL ANALYSIS

SUPPLEMENTAL INFORMATION

Supplemental information can be found online at https://doi.org/10.1016/j.celrep.2021.109564.

ACKNOWLEDGMENTS

The authors acknowledge the facilities and technical assistance of staff in the South Australian Health and Medical Research Institute (SAHMRI) bioresources and histology facilities. Flow cytometry analysis was performed at the ACRF Cellular Imaging and Cytometry Core Facility in SAHMRI. The ACRF Facility is generously supported by the Detmold Hoopman Group, Australian Cancer Research Foundation, and Australian Government through the Zero Childhood Cancer Program. The authors acknowledge the facilities and scientific and technical assistance of the National Imaging Facility, a National Collaborative Research Infrastructure Strategy (NCRIS) capability, at SAHRMI. We also acknowledge the SAHMRI genomics core for their assistance with RNA-seq and 16S rRNA library preparation and sequencing. We are grateful to Natalie Stevens and Todd Norton for assistance with some of the germ-free mouse experiments. This study was financially supported by an EMBL Australia Group Leader award (to D.J.L.).

AUTHOR CONTRIBUTIONS

D.J.L., G.B.R., and S.L.W. conceived of the study, which was performed under D.J.L.'s direction. M.A.L. performed the GF mouse experiments. M.A.L., G.E., and A.S. performed the majority of the SPF mouse work with assistance from S.C.B., J.J., T.C.Y., and S.J.B. FJ.R. performed the 16S rRNA sequencing and RNA-seq bioinformatics analyses with assistance from D.J.L. M.A.L., G.E., and J.M.C. performed the fecal DNA extractions and QC for 16S rRNA gene sequencing. J.B., X.W., L.S., and J.X. performed western immunoblotting under the supervision of C.G.P. The serum glucagon and serotonin assays were performed by E.W.S. and A.M.M. under the supervision of D.J.K. M.D.K. performed the EchoMRI. S.H. and J.B. performed brain histology, immunohistochemistry, and western blotting under the direction of T.J.S. M.A.L., F.J.R., and D.J.L. wrote the paper with contributions and final approval from all of the authors.

DECLARATION OF INTERESTS

The authors declare no competing interests.

Received: September 1, 2020
Revised: June 2, 2021
Accepted: July 29, 2021
Published: August 24, 2021

REFERENCES

Ainonen, S., Tejesvi, M.V., Mahmud, M.R., Paalanne, N., Pokka, T., Li, W., Nelson, K.E., Salo, J., Renko, M., Vänni, P., et al. (2021). Antibiotics at birth and later antibiotic courses: effects on gut microbiota. Pediatr. Res. Published online April 6, 2021. https://doi.org/10.1038/s41390-021-01494-7.

Al Nabhani, Z., Dulauroy, S., Marques, R., Cousu, C., Al Bounny, S., Déjardin, F., Sparwasser, T., Bérard, M., Cerf-Bensussan, N., and Eberl, G. (2019). A Weaning Reaction to Microbiota Is Required for Resistance to Immunopathologies in the Adult. Immunity *50*, 1276–1288.e5.

Aye, I.L., Jansson, T., and Powell, T.L. (2013). Interleukin-1β inhibits insulin signaling and prevents insulin-stimulated system A amino acid transport in primary human trophoblasts. Mol. Cell. Endocrinol. *381*, 46–55.

Bäckhed, F., Manchester, J.K., Semenkovich, C.F., and Gordon, J.I. (2007). Mechanisms underlying the resistance to diet-induced obesity in germ-free mice. Proc. Natl. Acad. Sci. USA *104*, 979–984.

Bahne, E., Sun, E.W.L., Young, R.L., Hansen, M., Sonne, D.P., Hansen, J.S., Rohde, U., Liou, A.P., Jackson, M.L., de Fontgalland, D., et al. (2018). Metformin-induced glucagon-like peptide-1 secretion contributes to the actions of metformin in type 2 diabetes. JCI Insight *3*, e93936.

Baldwin, S.L., Hsu, F.C., Van Hoeven, N., Gage, E., Granger, B., Guderian, J.A., Larsen, S.E., Lorenzo, E.C., Haynes, L., Reed, S.G., and Coler, R.N. (2018). Improved Immune Responses in Young and Aged Mice with Adjuvanted Vaccines against H1N1 Influenza Infection. Front. Immunol. *9*, 295.

Bárcena, C., Valdés-Mas, R., Mayoral, P., Garabaya, C., Durand, S., Rodríguez, F., Fernández-García, M.T., Salazar, N., Nogacka, A.M., Garatachea, N., et al. (2019). Healthspan and lifespan extension by fecal microbiota transplantation into progeroid mice. Nat. Med. *25*, 1234–1242.

Beli, E., Duriancik, D.M., Clinthorne, J.F., Lee, T., Kim, S., and Gardner, E.M. (2014). Natural killer cell development and maturation in aged mice. Mech. Ageing Dev. *135*, 33–40.

Biagi, E., Franceschi, C., Rampelli, S., Severgnini, M., Ostan, R., Turroni, S., Consolandi, C., Quercia, S., Scurti, M., Monti, D., et al. (2016). Gut Microbiota and Extreme Longevity. Curr. Biol. *26*, 1480–1485.

Bing, C. (2015). Is interleukin-1β a culprit in macrophage-adipocyte crosstalk in obesity? Adipocyte *4*, 149–152.

Biragyn, A., and Ferrucci, L. (2018). Gut dysbiosis: a potential link between increased cancer risk in ageing and inflammaging. Lancet Oncol. *19*, e295–e304.

Bokulich, N.A., Chung, J., Battaglia, T., Henderson, N., Jay, M., Li, H., Lieber, A.D., Wu, F., Perez-Perez, G.I., Chen, Y., et al. (2016). Antibiotics, birth mode, and diet shape microbiome maturation during early life. Sci. Transl. Med. *8*, 343ra82.

Bolger, A.M., Lohse, M., and Usadel, B. (2014). Trimmomatic: a flexible trimmer for Illumina sequence data. Bioinformatics *30*, 2114–2120.

Bolyen, E., Rideout, J.R., Dillon, M.R., Bokulich, N.A., Abnet, C.C., Al-Ghalith, G.A., Alexander, H., Alm, E.J., Arumugam, M., Asnicar, F., et al. (2019). Reproducible, interactive, scalable and extensible microbiome data science using QIIME 2. Nat. Biotechnol. *37*, 852–857.

Brace, L.E., Vose, S.C., Stanya, K., Gathungu, R.M., Marur, V.R., Longchamp, A., Treviño-Villarreal, H., Mejia, P., Vargas, D., Inouye, K., et al. (2016). Increased oxidative phosphorylation in response to acute and chronic DNA damage. NPJ Aging Mech. Dis. *2*, 16022.

Callahan, B.J., McMurdie, P.J., Rosen, M.J., Han, A.W., Johnson, A.J., and Holmes, S.P. (2016). DADA2: High-resolution sample inference from Illumina amplicon data. Nat. Methods *13*, 581–583.

Cani, P.D., Bibiloni, R., Knauf, C., Waget, A., Neyrinck, A.M., Delzenne, N.M., and Burcelin, R. (2008). Changes in gut microbiota control metabolic endotoxemia-induced inflammation in high-fat diet-induced obesity and diabetes in mice. Diabetes *57*, 1470–1481.

Chen, G., Lustig, A., and Weng, N.P. (2013). T cell aging: a review of the transcriptional changes determined from genome-wide analysis. Front. Immunol. *4*, 121.

Cho, I., Yamanishi, S., Cox, L., Methé, B.A., Zavadil, J., Li, K., Gao, Z., Mahana, D., Raju, K., Teitler, I., et al. (2012). Antibiotics in early life alter the murine colonic microbiome and adiposity. Nature *488*, 621–626.

Claesson, M.J., Jeffery, I.B., Conde, S., Power, S.E., O'Connor, E.M., Cusack, S., Harris, H.M., Coakley, M., Lakshminarayanan, B., O'Sullivan, O., et al. (2012). Gut microbiota composition correlates with diet and health in the elderly. Nature *488*, 178–184.

Clark, R.I., and Walker, D.W. (2018). Role of gut microbiota in aging-related health decline: insights from invertebrate models. Cell. Mol. Life Sci. *75*, 93–101.

Clark, R.I., Salazar, A., Yamada, R., Fitz-Gibbon, S., Morselli, M., Alcaraz, J., Rana, A., Rera, M., Pellegrini, M., Ja, W.W., and Walker, D.W. (2015). Distinct Shifts in Microbiota Composition during Drosophila Aging Impair Intestinal Function and Drive Mortality. Cell Rep. *12*, 1656–1667.

Copps, K.D., and White, M.F. (2012). Regulation of insulin sensitivity by serine/threonine phosphorylation of insulin receptor substrate proteins IRS1 and IRS2. Diabetologia *55*, 2565–2582.

Cox, L.M., and Blaser, M.J. (2015). Antibiotics in early life and obesity. Nat. Rev. Endocrinol. *11*, 182–190.

Cox, L.M., Yamanishi, S., Sohn, J., Alekseyenko, A.V., Leung, J.M., Cho, I., Kim, S.G., Li, H., Gao, Z., Mahana, D., et al. (2014). Altering the intestinal microbiota during a critical developmental window has lasting metabolic consequences. Cell *158*, 705–721.

DeJong, E.N., Surette, M.G., and Bowdish, D.M.E. (2020). The Gut Microbiota and Unhealthy Aging: Disentangling Cause from Consequence. Cell Host Microbe *28*, 180–189.

DeSantis, T.Z., Hugenholtz, P., Larsen, N., Rojas, M., Brodie, E.L., Keller, K., Huber, T., Dalevi, D., Hu, P., and Andersen, G.L. (2006). Greengenes, a chimera-checked 16S rRNA gene database and workbench compatible with ARB. Appl. Environ. Microbiol. *72*, 5069–5072.

Dethlefsen, L., and Relman, D.A. (2011). Incomplete recovery and individualized responses of the human distal gut microbiota to repeated antibiotic perturbation. Proc. Natl. Acad. Sci. USA *108* (*Suppl 1*), 4554–4561.

Douglas, G.M., Maffei, V.J., Zaneveld, J.R., Yurgel, S.N., Brown, J.R., Taylor, C.M., Huttenhower, C., and Langille, M.G.I. (2020). PICRUSt2 for prediction of metagenome functions. Nat. Biotechnol. *38*, 685–688.

Economopoulos, K.P., Ward, N.L., Phillips, C.D., Teshager, A., Patel, P., Mohamed, M.M., Hakimian, S., Cox, S.B., Ahmed, R., Moaven, O., et al. (2016). Prevention of antibiotic-associated metabolic syndrome in mice by intestinal alkaline phosphatase. Diabetes Obes. Metab. *18*, 519–527.

Erny, D., Hrabě de Angelis, A.L., Jaitin, D., Wieghofer, P., Staszewski, O., David, E., Keren-Shaul, H., Mahlakoiv, T., Jakobshagen, K., Buch, T., et al. (2015). Host microbiota constantly control maturation and function of microglia in the CNS. Nat. Neurosci. *18*, 965–977.

Ewels, P., Magnusson, M., Lundin, S., and Käller, M. (2016). MultiQC: summarize analysis results for multiple tools and samples in a single report. Bioinformatics *32*, 3047–3048.

Finch, C.E., and Girgis, F.G. (1974). Enlarged seminal vesicles of senescent C57BL-6J mice. J. Gerontol. *29*, 134–138.

Frasca, D., and Blomberg, B.B. (2016). Inflammaging decreases adaptive and innate immune responses in mice and humans. Biogerontology *17*, 7–19.

Fuchs, A., Bielicki, J., Mathur, S., Sharland, M., and Van Den Anker, J.N. (2016). Antibiotic Use for Sepsis in Neonates and Children: 2016 Evidence Update. https://www.who.int/selection_medicines/committees/expert/21/applications/s6_paed_antibiotics_appendix4_sepsis.pdf.

Galkin, F., Mamoshina, P., Aliper, A., Putin, E., Moskalev, V., Gladyshev, V.N., and Zhavoronkov, A. (2020). Human Gut Microbiome Aging Clock Based on Taxonomic Profiling and Deep Learning. iScience *23*, 101199.

Garigan, D., Hsu, A.L., Fraser, A.G., Kamath, R.S., Ahringer, J., and Kenyon, C. (2002). Genetic analysis of tissue aging in Caenorhabditis elegans: a role for heat-shock factor and bacterial proliferation. Genetics *161*, 1101–1112.

Han, B., Sivaramakrishnan, P., Lin, C.J., Neve, I.A.A., He, J., Tay, L.W.R., Sowa, J.N., Sizovs, A., Du, G., Wang, J., et al. (2017). Microbial Genetic Composition Tunes Host Longevity. Cell *169*, 1249–1262.e13.

Harrison, D.E., Strong, R., Sharp, Z.D., Nelson, J.F., Astle, C.M., Flurkey, K., Nadon, N.L., Wilkinson, J.E., Frenkel, K., Carter, C.S., et al. (2009). Rapamycin fed late in life extends lifespan in genetically heterogeneous mice. Nature *460*, 392–395.

Hassiotis, S., Manavis, J., Blumbergs, P.C., Hattersley, K.J., Carosi, J.M., Kamei, M., and Sargeant, T.J. (2018). Lysosomal LAMP1 immunoreactivity exists in both diffuse and neuritic amyloid plaques in the human hippocampus. Eur. J. Neurosci. *47*, 1043–1053.

Hay, N., and Sonenberg, N. (2004). Upstream and downstream of mTOR. Genes Dev. *18*, 1926–1945.

He, B., Liu, Y., Hoang, T.K., Tian, X., Taylor, C.M., Luo, M., Tran, D.Q., Tatevian, N., and Rhoads, J.M. (2019). Antibiotic-modulated microbiome suppresses lethal inflammation and prolongs lifespan in Treg-deficient mice. Microbiome *7*, 145.

Hildebrand, F., Moitinho-Silva, L., Blasche, S., Jahn, M.T., Gossmann, T.I., Huerta-Cepas, J., Hercog, R., Luetge, M., Bahram, M., Pryszlak, A., et al. (2019). Antibiotics-induced monodominance of a novel gut bacterial order. Gut *68*, 1781–1790.

Hofmann, J.W., Zhao, X., De Cecco, M., Peterson, A.L., Pagliaroli, L., Manivannan, J., Hubbard, G.B., Ikeno, Y., Zhang, Y., Feng, B., et al. (2015). Reduced expression of MYC increases longevity and enhances healthspan. Cell *160*, 477–488.

Jager, J., Grémeaux, T., Cormont, M., Le Marchand-Brustel, Y., and Tanti, J.F. (2007). Interleukin-1beta-induced insulin resistance in adipocytes through down-regulation of insulin receptor substrate-1 expression. Endocrinology *148*, 241–251.

Jernberg, C., Löfmark, S., Edlund, C., and Jansson, J.K. (2007). Long-term ecological impacts of antibiotic administration on the human intestinal microbiota. ISME J. *1*, 56–66.

Kim, D., Langmead, B., and Salzberg, S.L. (2015). HISAT: a fast spliced aligner with low memory requirements. Nat. Methods *12*, 357–360.

Knoop, K.A., Gustafsson, J.K., McDonald, K.G., Kulkarni, D.H., Coughlin, P.E., McCrate, S., Kim, D., Hsieh, C.S., Hogan, S.P., Elson, C.O., et al. (2017). Microbial antigen encounter during a preweaning interval is critical for tolerance to gut bacteria. Sci. Immunol. *2*, eaao1314.

Kong, F., Hua, Y., Zeng, B., Ning, R., Li, Y., and Zhao, J. (2016). Gut microbiota signatures of longevity. Curr. Biol. *26*, R832–R833.

Kundu, P., Lee, H.U., Garcia-Perez, I., Tay, E.X.Y., Kim, H., Faylon, L.E., Martin, K.A., Purbojati, R., Drautz-Moses, D.I., Ghosh, S., et al. (2019). Neurogenesis and prolongevity signaling in young germ-free mice transplanted with the gut microbiota of old mice. Sci. Transl. Med. *11*, eaau4760.

Labunskyy, V.M., Gerashchenko, M.V., Delaney, J.R., Kaya, A., Kennedy, B.K., Kaeberlein, M., and Gladyshev, V.N. (2014). Lifespan extension conferred by endoplasmic reticulum secretory pathway deficiency requires induction of the unfolded protein response. PLoS Genet. *10*, e1004019.

Leek, J.T. (2014). svaseq: removing batch effects and other unwanted noise from sequencing data. Nucleic Acids Res. *42*, e161.

Liang, W., Menke, A.L., Driessen, A., Koek, G.H., Lindeman, J.H., Stoop, R., Havekes, L.M., Kleemann, R., and van den Hoek, A.M. (2014). Establishment of a general NAFLD scoring system for rodent models and comparison to human liver pathology. PLoS ONE *9*, e115922.

Liao, Y., Smyth, G.K., and Shi, W. (2014). featureCounts: an efficient general purpose program for assigning sequence reads to genomic features. Bioinformatics *30*, 923–930.

Liberzon, A., Subramanian, A., Pinchback, R., Thorvaldsdóttir, H., Tamayo, P., and Mesirov, J.P. (2011). Molecular signatures database (MSigDB) 3.0. Bioinformatics *27*, 1739–1740.

Livanos, A.E., Greiner, T.U., Vangay, P., Pathmasiri, W., Stewart, D., McRitchie, S., Li, H., Chung, J., Sohn, J., Kim, S., et al. (2016). Antibiotic-mediated gut microbiome perturbation accelerates development of type 1 diabetes in mice. Nat. Microbiol. *1*, 16140.

Lynn, M.A., Tumes, D.J., Choo, J.M., Sribnaia, A., Blake, S.J., Leong, L.E.X., Young, G.P., Marshall, H.S., Wesselingh, S.L., Rogers, G.B., and Lynn, D.J. (2018). Early-Life Antibiotic-Driven Dysbiosis Leads to Dysregulated Vaccine Immune Responses in Mice. Cell Host Microbe *23*, 653–660.e5.

Martin, A.M., Yabut, J.M., Choo, J.M., Page, A.J., Sun, E.W., Jessup, C.F., Wesselingh, S.L., Khan, W.I., Rogers, G.B., Steinberg, G.R., and Keating, D.J. (2019). The gut microbiome regulates host glucose homeostasis via peripheral serotonin. Proc. Natl. Acad. Sci. USA *116*, 19802–19804.

Mayer, C.T., Tian, L., Hesse, C., Kühl, A.A., Swallow, M., Kruse, F., Thiele, M., Gershwin, M.E., Liston, A., and Sparwasser, T. (2014). Anti-CD4 treatment inhibits autoimmunity in scurfy mice through the attenuation of co-stimulatory signals. J. Autoimmun. *50*, 23–32.

Maynard, C., and Weinkove, D. (2018). The Gut Microbiota and Ageing. Subcell. Biochem. *90*, 351–371.

McDonald, J.U., Zhong, Z., Groves, H.T., and Tregoning, J.S. (2017). Inflammatory responses to influenza vaccination at the extremes of age. Immunology *151*, 451–463.

McDonnell, L., Gilkes, A., Ashworth, M., Rowland, V., Harries, T.H., Armstrong, D., and White, P. (2021). Association between antibiotics and gut microbiome dysbiosis in children: systematic review and meta-analysis. Gut Microbes *13*, 1–18.

McMurdie, P.J., and Holmes, S. (2013). phyloseq: an R package for reproducible interactive analysis and graphics of microbiome census data. PLoS ONE *8*, e61217.

Mulder, M., Radjabzadeh, D., Kiefte-de Jong, J.C., Uitterlinden, A.G., Kraaij, R., Stricker, B.H., and Verbon, A. (2020). Long-term effects of antimicrobial drugs on the composition of the human gut microbiota. Gut Microbes *12*, 1795492.

Murphy, E.F., Cotter, P.D., Hogan, A., O'Sullivan, O., Joyce, A., Fouhy, F., Clarke, S.F., Marques, T.M., O'Toole, P.W., Stanton, C., et al. (2013). Divergent metabolic outcomes arising from targeted manipulation of the gut microbiota in diet-induced obesity. Gut *62*, 220–226.

Nahata, M., Muto, S., Nakagawa, K., Ohnishi, S., Sadakane, C., Saegusa, Y., Iizuka, S., Hattori, T., Asaka, M., and Takeda, H. (2013). Serotonin 2C receptor antagonism ameliorates novelty-induced hypophagia in aged mice. Psychoneuroendocrinology *38*, 2051–2064.

Ng, K.M., Aranda-Díaz, A., Tropini, C., Frankel, M.R., Van Treuren, W., O'Loughlin, C.T., Merrill, B.D., Yu, F.B., Pruss, K.M., Oliveira, R.A., et al. (2019). Recovery of the Gut Microbiota after Antibiotics Depends on Host Diet, Community Context, and Environmental Reservoirs. Cell Host Microbe *26*, 650–665.e4.

Nobel, Y.R., Cox, L.M., Kirigin, F.F., Bokulich, N.A., Yamanishi, S., Teitler, I., Chung, J., Sohn, J., Barber, C.M., Goldfarb, D.S., et al. (2015). Metabolic and metagenomic outcomes from early-life pulsed antibiotic treatment. Nat. Commun. *6*, 7486.

O'Shea, A., Cohen, R.A., Porges, E.C., Nissim, N.R., and Woods, A.J. (2016). Cognitive Aging and the Hippocampus in Older Adults. Front. Aging Neurosci. *8*, 298.

Obata, F., Fons, C.O., and Gould, A.P. (2018). Early-life exposure to low-dose oxidants can increase longevity via microbiome remodelling in Drosophila. Nat. Commun. *9*, 975.

Palleja, A., Mikkelsen, K.H., Forslund, S.K., Kashani, A., Allin, K.H., Nielsen, T., Hansen, T.H., Liang, S., Feng, Q., Zhang, C., et al. (2018). Recovery of gut microbiota of healthy adults following antibiotic exposure. Nat. Microbiol. *3*, 1255–1265.

Pettan-Brewer, C., and Treuting, P.M. (2011). Practical pathology of aging mice. Pathobiol. Aging Age Relat. Dis. *1*.

Price, M.N., Dehal, P.S., and Arkin, A.P. (2010). FastTree 2–approximately maximum-likelihood trees for large alignments. PLoS ONE *5*, e9490.

Reynolds, T.H., Dalton, A., Calzini, L., Tuluca, A., Hoyte, D., and Ives, S.J. (2019). The impact of age and sex on body composition and glucose sensitivity in C57BL/6J mice. Physiol. Rep. *7*, e13995.

Robinson, M.D., McCarthy, D.J., and Smyth, G.K. (2010). edgeR: a Bioconductor package for differential expression analysis of digital gene expression data. Bioinformatics *26*, 139–140.

Rothschild, D., Leviatan, S., Hanemann, A., Cohen, Y., Weissbrod, O., and Segal, E. (2020). An atlas of robust microbiome associations with phenotypic traits based on large-scale cohorts from two continents. bioRxiv. https://doi.org/10.1101/2020.05.28.122325.

Sabatini, D.M. (2017). Twenty-five years of mTOR: Uncovering the link from nutrients to growth. Proc. Natl. Acad. Sci. USA *114*, 11818–11825.

Salazar, A.M., Resnik-Docampo, M., Ulgherait, M., Clark, R.I., Shirasu-Hiza, M., Jones, D.L., and Walker, D.W. (2018). Intestinal Snakeskin Limits Microbial Dysbiosis during Aging and Promotes Longevity. iScience *9*, 229–243.

Salosensaari, A., Laitinen, V., Havulinna, A., Meric, G., Cheng, S., Perola, M., Valsta, L., Alfthan, G., Inouye, M., Watrous, J.D., et al. (2020). Taxonomic Signatures of Long-Term Mortality Risk in Human Gut Microbiota. medRxiv. https://doi.org/10.1101/2019.12.30.19015842.

Scott, G.A., Terstege, D.J., Vu, A.P., Law, S., Evans, A., and Epp, J.R. (2020). Disrupted Neurogenesis in Germ-Free Mice: Effects of Age and Sex. Front. Cell Dev. Biol. *8*, 407.

Shavlakadze, T., Morris, M., Fang, J., Wang, S.X., Zhu, J., Zhou, W., Tse, H.W., Mondragon-Gonzalez, R., Roma, G., and Glass, D.J. (2019). Age-Related Gene Expression Signature in Rats Demonstrate Early, Late, and Linear Transcriptional Changes from Multiple Tissues. Cell Rep. *28*, 3263–3273.e3.

Smith, P., Willemsen, D., Popkes, M., Metge, F., Gandiwa, E., Reichard, M., and Valenzano, D.R. (2017). Regulation of life span by the gut microbiota in the short-lived African turquoise killifish. eLife *6*, e27014.

Smith, B.J., Miller, R.A., Ericsson, A.C., Harrison, D.C., Strong, R., and Schmidt, T.M. (2019). Changes in the gut microbiome and fermentation products concurrent with enhanced longevity in acarbose-treated mice. BMC Microbiol. *19*, 130.

Taylor, D.N. (2005). Poorly absorbed antibiotics for the treatment of traveler's diarrhea. Clin. Infect. Dis. *41* (*Suppl 8*), S564–S570.

Thevaranjan, N., Puchta, A., Schulz, C., Naidoo, A., Szamosi, J.C., Verschoor, C.P., Loukov, D., Schenck, L.P., Jury, J., Foley, K.P., et al. (2017). Age-Associated Microbial Dysbiosis Promotes Intestinal Permeability,

Systemic Inflammation, and Macrophage Dysfunction. Cell Host Microbe *21*, 455–466.e4.

Tian, S., Wang, X., and Proud, C.G. (2017). Oncogenic MNK signalling regulates the metastasis suppressor NDRG1. Oncotarget *8*, 46121–46135.

Virk, B., Correia, G., Dixon, D.P., Feyst, I., Jia, J., Oberleitner, N., Briggs, Z., Hodge, E., Edwards, R., Ward, J., et al. (2012). Excessive folate synthesis limits lifespan in the C. elegans: E. coli aging model. BMC Biol. *10*, 67.

White, R.R., Milholland, B., MacRae, S.L., Lin, M., Zheng, D., and Vijg, J. (2015). Comprehensive transcriptional landscape of aging mouse liver. BMC Genomics *16*, 899.

Whyte, L.S., Hassiotis, S., Hattersley, K.J., Hemsley, K.M., Hopwood, J.J., Lau, A.A., and Sargeant, T.J. (2020). Lysosomal Dysregulation in the Murine App$^{NL-G-F/NL-G-F}$ Model of Alzheimer's Disease. Neuroscience *429*, 143–155.

Wickham, H. (2016). ggplot2: Elegant Graphics for Data Analysis. (Springer).

STAR★METHODS

KEY RESOURCES TABLE

REAGENT or RESOURCE	SOURCE	IDENTIFIER
Antibodies		
Goat anti-Mouse IgG (H+L) Secondary Antibody, HRP conjugate	Life Technologies	Cat#A16066; RRID:AB_2534739
CD19 (Clone 1D3)	BD	Cat#550284; RRID:AB_393579
Nk1.1 (Clone PK136)	BD	Cat#550627; RRID:AB_398463
B220 (Clone RA3-6B2)	BD	Cat#552772; RRID:AB_394458
TCR-B (Clone H57-597)	BD	Cat#560729; RRID:AB_1937310
CD11b (Clone M1/70)	BD	Cat#563168; RRID:AB_2716860
CD11c (Clone HL3)	BD	Cat#561241; RRID:AB_10611727
MHC class II (Clone M5/114.15.2)	Miltenyi Biotec	Cat# 130-091-368; RRID:AB_615137
CD8 (Clone 53-6.7)	BD	Cat#563786; RRID:AB_2732919
CD44 (Clone IM7)	BD	Cat#550538; RRID:AB_393732
CD73 (Clone TY/23)	BD	Cat#550741; RRID:AB_393860
CD4 (clone RM4-5)	Biolegend	Cat#100505; RRID:AB_312708
CD62L (clone MEL14-H2.100)	Miltenyi Biotec	Cat#130-102-465; RRID:AB_2660513
Ly6G (clone1A8)	Miltenyi Biotec	Cat#130-101-884; RRID:AB_2660052
CD209 (REA125)	Miltenyi Biotec	Cat#130-106-329; RRID:AB_2656271
CD279 (Clone REA802)	Miltenyi Biotec	Cat#130-111-954; RRID:AB_2656935
TNFα (Clone MP6-XT22)	Miltenyi Biotec	Cat#130-102-294; RRID:AB_2661140
Anti-phospho-S6 Ser240/S244	Cell Signaling Technology	Cat#5364; RRID:AB_10694233
Ribosomal Protein S6 (C-8)	Santa Cruz Biotechnology	Cat#SC-74459; RRID:AB_1129205
IRS1	Millipore	Cat#06-248; RRID:AB_2127890
Anti-GAPDH Antibody	Abcam	Cat#Ab-9485; RRID:AB_307275
Anti-IBA1, Rabbit	Fujifilm Wako Pure Chemical Corporation	Cat#016-20001; RRID:AB_839506
Anti-Doublecortin, Rabbit	Jackson Immunoresearch Laboratories	Cat#Ab18723; RRID:AB_732011
Biotinylated secondary antibody donkey anti-rabbit IgG	Jackson Immunoresearch Laboratories	Cat#711-065-152; RRID:AB_2340593
CD45.2 clone (104)	BD	Cat#560694; RRID:AB_1727492
CD3 clone (REA641)	Miltenyi Biotec	Cat#130-120-826; RRID:AB_2752207
CD8 clone (53-6.7)	BD	Cat#563786; RRID:AB_2732919
IFNγ clone (XMG1.2)	BD	Cat#554411; RRID:AB_395375
Chemicals, peptides, and recombinant proteins		
Ampicillin sodium salt	Sigma Aldrich	Cat#A0166
Neomycin trisulfate salt hydrate	Sigma Aldrich	Cat#N1876
Actrapid Human Insulin	Novo Nordisk Pharmaceuticals	N/A
Afluria Quad™	Seqirus	N/A
eBioscience ELISA/ELISPOT Diluent 5x	Thermo Fisher Scientific	Cat#00-4202-56
TRIzol Reagent	Life Technologies	Cat#15596026
Glycogen	Thermo Fisher Scientific	Cat#R0561
DNase I (for RNA extractions)	Life Technologies	Cat#18068015
Protoscript II	NEB	Cat#E6560S
BD Pharm Lyse	BD	Cat#555899
RPMI1640	Sigma-Aldrich	Cat#R8758
Fetal Bovine serum (French origin)	Assay Matrix, Australia	Cat#ASFBS-FR
MEM Non-Essential Amino Acids Solution (100X)	Thermofisher	Cat#11140050

(*Continued on next page*)

Continued

REAGENT or RESOURCE	SOURCE	IDENTIFIER
GlutaMAX Supplement	Thermofisher	Cat#35050079
penicillin/streptomycin	GIBCO	Cat#15140122
LPS	Sigma	Cat#L2880-10MG
Phorbol 12-myristate 13-acetate	Sigma	Cat#P8139-1MG
Ionomycin calcium salt from *Streptomyces conglobatus*	Sigma	Cat#I0634-1MG
GolgiPlug Protein Transport Inhibitor	BD	Cat#555029
Roche protease inhibitor cocktail	Sigma-Aldrich	Cat#04693132001
Collagenase IV	GIBCO	Cat#17104019
DNase I	Roche Diagnostic	Cat#11284932
Percoll	Biostrategy	Cat#GEHE17-0891-01
Critical commercial assays		
Freestyle Optium Blood Ketone strips	Abbott	Cat#MV99113
Freestyle Optium Glucose Strips	Abbott	Cat#MV99884
Ultra-Sensitive Mouse Insulin ELISA Kit	eBioscience	Cat#88-50400
IFN gamma Mouse ELISA kit	Thermo Fisher Scientific	Cat#88-7314-88
IL-1 beta Mouse Uncoated ELISA kit	Thermo Fisher Scientific	Cat#88-7013-77
TNF alpha Mouse Uncoated ELISA kit	Thermo Fisher Scientific	Cat#88-7324-77
Glucagon ELISA - 10 μL	Mercodia	Cat#10-1281-01
Serotonin (5-HT) ELISA kit	Labor Diagnostika	Cat#BA E-5900
Fixation and Permeabilization Solution	BD	Cat#554722
Vectastain Elite ABC Kit	Vector Laboratories	Cat#PK6100; RRID:AB_2336819
Peroxidase-conjugated Streptavidin	Jackson Immunoresearch Laboratories	Cat#016-030-084
DAKO liquid DAB chromogen kit	DAKO	Cat#K346811
Deposited data		
16S rRNA gene Sequence Data	This paper	SRA BioProject: PRJNA645716
RNA-Seq data	This paper	GEO: GSE154465
R code for analysis and plots	Bitbucket	https://bitbucket.org/lynnlab/longevity
Experimental models: Organisms/strains		
C57BL/6J	The Jackson Laboratory	Cat#000664
C57BL/6J germ-free mice	Translational Research Institute, QLD, AU	N/A
Oligonucleotides		
Irs1 Fwd 5«CCTTTCCTTGTTTGAAAGGTCGATA –3	This paper	N/A
Irs1 Rev 5«CCAACCAGTTGATCAGGGCA –3	This paper	N/A
Ifng primers	QIAGEN	Cat#PPM03121A
Tnfa primers	QIAGEN	Cat#PPM03113G
Hsp90 Fwd 5«TTGGTTACTTCCCCGTGCTG –3	This paper	N/A
Hsp90 Rev 5« GCCTTTTGCCGTAGGGTTTC –3	This paper	N/A
Gapdh Fwd 5«CTCCCACTCTTCCACCTTCG –3	This paper	N/A
Gapdh Rev 5«GCCTCTCTTGCTCAGTGTCC –3	This paper	N/A
Hrpt Fwd 5«CTGGTGAAAAGGACCTCTCGAAG –3	This paper	N/A
Hrpt Rev 5«CCAGTTTCACTAATGACACAAACG-3	This paper	N/A
Software and algorithms		
GraphPad Prism 7.01	GraphPad Software Inc	version 7.01
FlowJo software	Tree Star	version 10.6.1
Case Viewer Program	3D Histech	version 2.0
MultiQC	Ewels et al., 2016	version 1.8
FastQC	Babraham Bioinformatics	version 0.11.4
Trimmomatic	Bolger et al., 2014	version 0.38

(*Continued on next page*)

Continued

REAGENT or RESOURCE	SOURCE	IDENTIFIER
HiSAT2	Kim et al., 2015	version 2.1.0
FeatureCounts	Liao et al., 2014	version 1.5.0-p2
R	R Core Team	version 3.6.3
SVASeq	Leek, 2014	version 3.3
QIIME2	Bolyen et al., 2019	version 2019.10
EdgeR	Robinson et al., 2010	version 3.26
ggplot2	Wickham. 2016	version 3.3
PICRUSt2	Douglas et al., 2020	version 2.3

RESOURCE AVAILABILITY

Lead contact

Further information and requests for resources and reagents should be directed to and will be fulfilled by the Lead Contact, David Lynn (david.lynn@sahmri.com).

Materials availability

This study did not generate new unique reagents.

Data and code availability

- The 16S rRNA gene sequence data have been deposited at NCBI Sequence Read Archive under BioProject: PRJNA645716 and the RNA-Seq data have been deposited in the Gene Expression Omnibus (GEO): GSE154465 and are publicly available as of the date of publication.
- All original code has been deposited at the Lynn Laboratory Bitbucket repository (https://bitbucket.org/lynnlab/longevity).
- Any additional information required to reanalyze the data reported in this paper is available from the lead contact upon request.

EXPERIMENTAL MODEL AND SUBJECT DETAILS

C57BL/6J (RRID:IMSR_JAX:000664) mice were bred and maintained under specific and opportunistic pathogen free conditions at the South Australian Health and Medical Research Institute (SAHMRI). All mice had access *ad libitum* to commercial food pellets (2018 Teklad global 18% protein, Envigo) and water. Standardized housing conditions were maintained with 12 h day/night cycle as well as regulated temperature and humidity. All experimental procedures were approved by the SAHMRI Animal Ethics Committee. Male mice were followed from birth to week 102 of life. Aged mice were humanely killed at 102 weeks of age. Young adult mice (12 weeks of age; n = 15) were humanely killed in parallel for comparison with aged mice.

Gnotobiotic (germ free) C57BL/6J mice (male and female; from birth to day 21 of age), (Translational Research Institute, QLD, AU) were housed in positively pressurised, high-efficiency particulate air (HEPA) filtered isolators, at the SAHMRI Preclinical, Imaging and Research Laboratories (PIRL) with access to autoclaved commercially pelleted food and sterilized water *ad libitum* with regulated daylight, humidity, and temperature.

METHOD DETAILS

Antibiotics

Pregnant dams (n = 6/group) were selected from the same breeding colony and randomly assigned to antibiotic treatment. All dams were 8-12 weeks of age and were in their first gestation. There were n = 20 unexposed control pups (No ABX) and n = 20 antibiotic exposed pups (ABX). Post-weaning, male littermates were randomly assigned to different cages (n = 5/cage). The investigators were not blinded to the experimental groups. Antibiotics (1 g/L ampicillin (Sigma, Darmstadt, Germany) and 0.5g/L neomycin (Sigma) were administered to assigned pregnant dams via the drinking water; commencing approximately 14 days post-coitus (E14) until 21 days after birth (D21). Antibiotics were replenished every 3 days during the specified period. Ampicillin and neomycin represent two classes of antibiotic that are administered to infants with suspected sepsis (Fuchs et al., 2016), though they would not usually be administered orally and our model uses a supra-clinical dose of neomycin. Neomycin has the added advantage in that it is poorly absorbed outside the gut and therefore oral administration targets the gut microbiota (Taylor, 2005).

Germ-free mouse experiments

Individual fecal samples collected from PAM I and PAM II mice at day 28 post-birth were pooled and resuspended in 15% glycerol using a Stomacher (Thomas Scientific) under anaerobic conditions. 100 μL of PAM I or PAM II faecal slurry was administered to germ-free mice via oral gavage at day 14 of life.

Body composition scanning – EchoMRI

Aged mice (96 weeks old) were imaged using an EchoMRI (Whole Body Composition Analyzers, Houston, USA) to determine body composition as per manufacturer's instructions. The EchoMRI measures whole body fat, lean and free water in live mice. All values were normalized for body weight.

Insulin and glucose tolerance test

Aged mice were subjected to an insulin (ITT) and glucose tolerance test (GTT) at approximately 95 weeks of age. Mice were fasted for 5-6 hours with free access to water. The ITT was conducted at least one week prior to the GTT. Baseline blood glucose and ketone levels were measured from the tail vein blood using a glucometer (Abbott Diabetes Care; Freestyle Optium Neo, California, USA). Mice were injected intraperitoneally with 0.75 IU/kg body weight of Actrapid® human insulin (Novo Nordisk Pharmaceuticals, Australia) (ITT) or 2 mg/kg glucose solution (Sigma) (GTT). Blood glucose levels were monitored at 15, 30, 60 and 120 min post-injection. Serum insulin was also measured during the GTT using a commercial ELISA kit (Crystal Chem, Ultra Sensitive Mouse Insulin ELISA Kit, Illinois, USA).

Fecal sampling

Mice had fecal pellets collected at least once every 3 months for the duration of the experiments. Fecal pellets were aseptically collected, immediately snap-frozen and stored at −80°C.

DNA extraction from fecal samples

Fecal samples were individually weighed, re-suspended in 1 mL of phosphate buffered saline (PBS) (pH 7.2) by vortexing, and pelleted by centrifugation at 13,000 x g for 5 min. DNA extraction was performed on the fecal pellets using a DNeasy PowerSoil Kit (QIAGEN, Hilden, Germany) with the following minor modifications; fecal pellets were re-suspended in 750 μL of Powersoil® bead solution and 60 μL solution C1 in a Powersoil® bead plate and incubated at 65°C for 10 min prior to bead beating. Subsequent DNA extraction procedures were performed according to the manufacturer's instructions.

16S rRNA gene sequence analysis

16S rRNA gene sequencing was conducted on fecal samples aseptically collected from individual mice at weeks 4, 72, 84, 96 and 102 of life. Fecal samples collected in the intervening weeks were pooled and sequenced. Fecal DNA extracts were used to generate amplicons of the V4 hypervariable region of the 16S rRNA gene as described previously (Lynn et al., 2018). Sequencing of the amplicon library was performed using an Illumina Miseq system (2 × 300bp run). Paired end 16S rRNA gene sequences were demultiplexed and imported into QIIME2 (release 2019.9) for processing (Bolyen et al., 2019). Sequences were error corrected, and counts of error-corrected reads per sample, which we refer to herein as exact sequence variants (ESVs), were generated with DADA2 version 1.8 (Callahan et al., 2016). A phylogenetic tree of error-corrected sequences was constructed with FastTree (Price et al., 2010). Taxonomy was assigned to sequences with the sklearn plugin for QIIME2 with an 80% confidence threshold, using the GreenGenes 13.8 database (DeSantis et al., 2006). MetaCyc pathway relative abundance was predicted using PICRUSt2 (Douglas et al., 2020). Further statistical analysis was carried out in R version 3.6.3, with graphing performed using ggplot2 (Wickham, 2016). Alpha and Beta diversity values were generated using PhyloSeq version 1.3 (McMurdie and Holmes, 2013).

Vaccination

Mice were immunized subcutaneously with 100 μL of the seasonal influenza vaccine (Afluria Quad 2019, Seqirus, Parkville, Australia) at 84 weeks of age. Young adult mice (8 weeks old) were immunized or mock vaccinated in parallel with 100 μL of PBS (s.c.). Serum was collected prior to vaccination/mock vaccination and at pre-determined time points post-vaccination.

Antibody response

Antigen-specific total IgG were measured by ELISA using Nunc MaxiSorp® ELISA plates (ThermoFisher) that were coated with Afluria quad™ vaccine (Seqiris) at 1 in 50 and incubated overnight at 4°C. Plates were washed once with 0.5% Tween-20/PBS (Sigma) and blocked with 1 X ELISA buffer (eBioscience, Waltham, USA). Mouse serum samples were diluted in 1X ELISA buffer and incubated on blocked plates. Antigen-specific serum antibodies were detected using horseradish peroxidase (HRP) conjugated antibodies anti-mouse IgG (Novex, Lake Oswego, USA) at a dilution of 1:1000. HRP activity was detected using tetramethylbenzidine (TMB) substrate (ThermoFisher) and stopped with 2N H_2SO_4. Developed plates were recorded using a microplate absorbance reader at 450 nm with correction at 595 nm by subtraction. Total IgG was also measured using an IgG ELISA kit according to the manufacturer's instructions (eBioscience, Waltham, USA).

Cytokine analysis

Serum was collected from mice at 60, 84 and 92 weeks of age. Serum was also collected from young adult mice (12 weeks). IFNγ, TNFα and IL-1β levels were assessed by ELISA (ThermoFisher).

Measurements of serum glucagon and serotonin

Serum glucagon was measured by ELISA (Bahne et al., 2018) as per manufacturer's instructions (Mercodia, Sweden). Serum 5-HT was measured by Ultra-Sensitive ELISA (BA E-5900; Labor Diagnostika Nord, Germany) as per manufacturer's instructions, at a 1:10,000 dilution in diluent buffer. Absorbance was read at 450 nm using a plate reader (Beckmann DTX 880), with a background reference of 620 nm.

RNA extraction

Tissue portions from liver and muscle were snap frozen and 50 mg sections were resuspended in TRIzol (ThermoFisher) and homogenized with a stainless-steel bead (5 mm) using a TissueLyser II (QIAGEN) for 2 min at 30 Hz. 20 mm ileum sections were ground with a mortar and pestle prior to resuspension in TRIzol. To extract RNA, 0.2 mL chloroform (Sigma, Australia) was added per 500 μL of TRIzol reagent and mixed vigorously for 15 s. The suspension was spun at 12,000 x g for 15 min to separate the aqueous and organic layers. The upper layer (containing the RNA) was collected and an isopropanol precipitation reaction was performed. Briefly, 5 μg of glycogen (Life technologies, Waltham, USA) and 0.25 mL of 100% isopropanol (Sigma, Australia) were added to the upper layer and incubated for 10 min. A pellet formed when the suspension was spun at 15,000 x g for 30 min. The pellet was washed twice in 75% ethanol and resuspended in 50 μL of RNase-free water. All RNA samples were treated with DNase (Life Technologies) to remove any contaminating DNA from the purified RNA. Briefly, 2 Units/μL of rDNase I enzyme was added to RNA in 10X DNase I Buffer and incubated at 37°C for 30 min. The reaction was inactivated by addition of DNase Inactivation Reagent and purified DNA-free RNA was ethanol precipitated from the resultant supernatant. RNA quality was confirmed using nanodrop (ThermoFisher) and RNA 6000 Nano Kit (Agilent) and Qubit RNA BR Assay Kit (ThermoFisher).

RT-qPCR

cDNA was prepared from purified gastrocnemius muscle and ileum RNA as per manufacturer's instructions (New England Biolabs). Briefly, 1μg of extracted RNA, 0.5μg/μL Oligo dT's (Life Technologies) and 10mM dNTP's (Life Technologies) was added to a final volume of 12μL nuclease-free water. RNA solution was then denatured using a heating block at 65°C for 5 min. Following denaturation 4 μL 5X ProtoScript II buffer, 2 μL 0.1M DTT and 0.7 μL ProtoScript II Reverse Transcriptase (New England Biolabs, Ipswich, USA) were added to samples. The reaction was incubated at 42°C for 60 min and then at 65°C for 20 min.

To determine relative mRNA expression, cDNA was diluted 10X in nuclease-free water. *Irs1*, *Gapdh, Tnfa, Ifng, Hprt and Hsp90* were amplified. Each reaction consisted of 5 μL SYBR Green PCR Master Mix (Life Technologies, Australia), 0.2 μM of each forward and reverse primer and 3 μL DNA template, diluted in sterile water to a total reaction volume of 10 μL. A no template DNA control, with the DNA substituted for 1 μL sterile water, was included in each run. A real-time PCR reaction of each sample was performed in duplicate, consisting of 10 μL per reaction. The amplification program was 50°C for 2 min, 95°C for 10 min, followed by 40 cycles at 95°C for 15 s and 60°C for 1 min. A melting curve analysis was performed at the end of the program. *Irs1* values were normalized to *Gapdh*. For the *Ifng* and *Tnfα* quantitative RT-PCR, Ct values were normalized to the mean Ct obtained from three house-keeping genes (*Gapdh*, *Hprt*, and *Hsp90*) in each sample.

Liver RNA-Seq analysis

Total liver RNA was converted to strand specific Illumina compatible sequencing libraries using the Universal Plus mRNA mRNA-Seq library kit from Tecan (Mannedorf, Switzerland) as per the manufacturer's instructions (MO1442 v2). Briefly, 400 ng of total RNA was polyA selected and the mRNA fragmented prior to reverse transcription and second strand cDNA synthesis. The resultant cDNA was end repaired before the ligation of Illumina-compatible barcoded sequencing adapters. The cDNA libraries were strand selected and PCR amplified for 14 cycles. Libraries were assessed using an Agilent Tapestation. A Qubit fluorescence assay was used to quantify the libraries (ThermoFisher). Sequencing pools were generated by mixing equimolar amounts of compatible sample libraries based on the Qubit measurements. Sequencing of the library pool was done with an Illumina Novaseq 6000 using a S1 flowcell with 2x100bp paired-end reads.

Sequence read quality was assessed using FastQC version 0.11.4 and summarized with MultiQC version 1.8 (Ewels et al., 2016) prior to quality control with Trimmomatic version 0.38 (Bolger et al., 2014) with a window size of 2 and an average quality score of 20. Following this, reads which were < 50c nucleotides after trimming were discarded. Reads that passed all quality control steps were then aligned to the mouse genome (GRCm38 assembly) using HISAT2 version 2.1.0 (Kim et al., 2015) . The gene count matrix was generated with FeatureCounts version 1.5.0-p2 (Liao et al., 2014) using the union model with Ensembl version 99 annotation. This was then imported into R version 3.6.3 for further analysis. Counts were normalized using the trimmed mean of M values (TMM) method in EdgeR version 3.28.1 (Robinson et al., 2010) prior to multidimensional scaling analysis and differential gene expression analysis (as performed with the glmLRT function). Unknown sources of variation were adjusted using SVASeq (Leek, 2014). Genes with < 1 count per million (cpm) in 3 samples were discarded prior to differential expression analysis. Gene set enrichment analysis was carried out using the MSigDB v7.1 gene sets (Liberzon et al., 2011) with the Camera function in the EdgeR package (v3.26.5).

Pathway over representation analysis was performed using a hypergeometric test in R with Gene Ontology and pathway data from R libraries biomaRt (v2.4), GO.db (v3.8.2), reactome.db (v1.68) and KEGGREST (v1.24). Complete R code for the analysis is accessible as per the data availability statement.

Splenocyte preparation

Single cell suspensions of spleen cells were prepared by mechanical dissociation and filtration through an 80 μm nylon filter (Merck Millipore, Darmstadt, Germany). Red blood cells were lysed with BD Pharm Lyse (BD Biosciences, San Jose, USA). Spleen cells (100 mL of a 10^7 cells/mL suspension) were plated in 96 well flat-bottom tissue culture plates (Costar, Corning, USA) in culture media consisting of RPMI1640 (Sigma-Aldrich) supplemented with 1% fetal calf serum (Assay Matrix, Australia).

Immunofluorescent staining for splenocyte flow cytometric analysis

Flow cytometry data was acquired on an LSRFortessa X-20 flow cytometer using FACSDiva software (BD Biosciences, New Jersey, USA) and results analyzed using the FlowJo software (Tree Star, Ashland, USA). Anti-mouse antibodies used for cell surface staining were CD19, NK1.1, B220, TCR-B, CD11b, CD11c, MHC2, CD8, CD44, CD73 all from BD; CD4 from Biolegend; and CD62L, Ly6G, CD209, CD279, TNFα, all from Miltenyi.

Blood and spleen stimulations

200 ul of peripheral blood was collected from GF, GF+PAM I, GF+ PAM II and SPF mice at day 21. Red blood cells were lysed with BD Pharm Lyse (BD Biosciences, San Jose, USA). Cells were stimulated with 10 ng/mL LPS (Sigma-Aldrich) for 18 hours. Splenocytes were prepared as described (Splenocyte preparation). Spleen cells (100 μL of a 1×10^7 cells/ml suspension) were plated in 96 well flat bottom tissue culture plates (Costar, Corning, USA) in culture media consisting of RPMI1640 (Sigma) supplemented with 10% fetal calf serum (Assay Matrix, Australia), Penicillin/streptomycin, Minimal essential media amino acids, and GlutaMAX Lglutamine (Thermofisher) added to the manufacturers' recommendation, and 2-Mercaptoethanol to a final concentration of 55nM (Life Technologies). Cells were stimulated with 10 ng/mL LPS (Sigma-Aldrich) for 18 hours.

Protein extraction from muscle and liver

20 mg muscle or liver was homogenized using Precellys 24 (Bertin) in RIPA lysis buffer (50 mM Tris-HCl, pH 7.5, 150 mM NaCl, 1% (v/v) NP-40 (IGEPAL CA-630), 0.1% (v/v) sodium deoxycholate, 0.1% (v/v) sodium dodecyl sulfate (SDS), 1 mM ethylenediaminetetra-acetic acid (EDTA), 50 mM β-glycerophosphate, 50 mM NaF, 5 mM $H_2Na_2P_2O_7$, 0.5 mM $NaVO_3$, 0.1% (v/v) 2-mercaptoethanol (Sigma) and protease inhibitor cocktail (Roche, purchased through Sigma-Aldrich)) at 4°C. Program setting: 6500 rpm, 2 × 20 s, 20 s interval. The homogenized lysates were incubated at RT for 5 min followed by centrifugation at 12,000 rpm for 1 min at 4°C. After transferring the lysates to new Eppendorf tubes, lysates were centrifuged at 13,200 rpm for 10 min at 4°C. Supernatants were then transferred to new tubes. Protein content was determined by the Bradford protein assay and equal amount of proteins were loaded on SDS-PAGE.

Western immunoblotting

For western blots, nitrocellulose membranes were probed with primary antibody in PBST with 5% BSA (w/v) overnight at 4°C, then incubated with fluorescently-tagged secondary antibody in PBST for 1 hour, rinsed, visualized and quantified using the Odyssey® Quantitative Imaging System (LI-COR) (Tian et al., 2017). GAPDH was used as a loading control. Antibodies used: P-S6 (S240/S244, Cell Signaling Technology 5364), S6 (Santa Cruz 74459), GAPDH (Abcam 9485), IRS1 (Millipore 06-148).

Liver histology

Portions of the liver were fixed in 10% neutral buffered formalin (POCD Scientific) for 7 days and transferred to an 80% ethanol solution for storage. Liver sections were embedded in a paraffin block and lateral cross-sections were cut and stained with hematoxylin and eosin (Histology Services, University of Adelaide, SA, AU). Slides were then scanned using a SCN400 F Brightfield and Fluorescence Slide Scanner (Leica Microsystems, Wetzlar, DEU) at 20X magnification and the CaseViewer software (3DHISTECH Ltd) was used to visualize samples. The severity of steatosis (Liang et al., 2014) and inflammation (Mayer et al., 2014) the liver was scored across specimens in a blinded fashion according to the following definitions. The liver score is the sum of individual scores for steatosis: macrovesicular steatosis, microvesicular steatosis and hypertrophy and individual scores for inflammatory; portal inflammation, lobular inflammation and necrosis. Individual scores were given as follows; macrovesicular steatosis, microvesicular steatosis and hypertrophy: 0, < 5%; 1, 5%–33% 2, 34%–66%; 3, > 66%. Portal, lobular and necrosis inflammation: 0, no inflammatory infiltrate; 1, low level of inflammatory cell infiltration; 2, moderate level of inflammatory cell infiltration; 3, severe inflammation.

Brain histology and immunohistochemistry

Half brains were post-fixed with 10% neutral buffered formalin (ThermoFisher) for routine paraffin embedment as previously described (Whyte et al., 2020). Six-micron paraffin sections of mouse brain were cut using a Leica microtome (RM2235) and subjected to immunohistochemical staining for Ionized calcium binding adaptor molecule 1, IBA-1 (FUJIFILM Wako Pure Chemical Corporation) and Doublecortin DCX (Abcam) (Hassiotis et al., 2018). Briefly, sections were dewaxed and rehydrated prior to microwave

heat-induced epitope retrieval using 0.01 M citrate buffer, 0.05% Tween 20, pH 6.0 (20 mins for Iba-1; 10 mins for DCX). Following blocking of non-specific proteins in 10% normal donkey serum for 2 hours, primary antibodies (rabbit anti-IBA-1 1:500, rabbit anti-DCX 1:5000) were applied overnight at room temperature. Sections were then treated with 0.3% hydrogen peroxide in PBS for 30 minutes followed by incubation with biotinylated donkey anti-rabbit (1:2000) for 1 hour prior to conjugation with avidin (Vectastain Elite ABC Kit for IBA-1; Peroxidase-conjugated Streptavidin for DCX) and visualization with DAKO liquid DAB chromogen kit (DAKO). Stained slides were counterstained with hematoxylin. All slides were dehydrated, cleared and a coverslip was applied. Negative controls for immunoreactivity were included by omission of each primary antibody for each batch run. All other steps in the procedure remained the same.

Brain image analysis and assessment of immunohistochemistry

All imaging and subsequent analysis was carried out with the operator blinded to treatment status. Immunohistochemically stained IBA-1 sections were scanned at 40X magnification using the Panoramic 250 Flash II slide scanner and viewed with the CaseViewer Program (3D Histech). Using the annotation tool in the Case Viewer Program, the dentate gyrus region was outlined (average area of 0.45mm^2). The number of IBA-1-positive cells in this region was manually counted in the CaseViewer Program and data were reported as number of positive cells per mm^2. Immunohistochemically stained DCX slides were viewed using the Olympus BX41 brightfield microscope and the dentate gyrus region was qualitatively assessed for the presence of DCX-positive neurons.

Lamina propria preparation

Small intestinal lamina propria cells were isolated as previously described (Al Nabhani et al., 2019). Briefly, Peyer's patches were removed and the small intestine was opened longitudinally and washed extensively with RPMI with 3% FBS and 2 mM EDTA and cut into sections. Intestinal sections were initial incubated with DTT (Sigma-Aldrich) for 10 mins at 37°C and spun at 800 x g and epithelial layer was discarded. Intestinal sections were digested with Collagenase IV (Thermofisher) and DNase I (Roche diagnostics, North Ryde, Australia) for 15- 35 min at 37°C and filtered through 40 μM cell strainers to generate single cell suspensions. Cells were separated by a 44/66% (w/v) Percoll density gradient (Biostrategy, Tingalpa, Australia). Isolated gut lamina propria cells were stimulated with 50 mg/mL PMA and 500 ng/mL ionamycin and 1x Brefeldin A (BD) for 4 hours in complete media at 37°C 5% CO_2.

Immunofluorescent staining for lamina propria cytometric analysis

Stimulated lamina propria cells were surface stained with CD45.2, CD3, CD4 and CD8. Stained cells were fixed and permeabilised with Fixation/permeabilization buffer (BD, Macquarie Park, Australia) and intracellular stained for IFNγ and TNFα.

QUANTIFICATION AND STATISTICAL ANALYSIS

Statistical analysis as detailed in the figure legends was performed in GraphPad Prism 7.01 (GraphPad Software Inc., CA, USA). The figure legends state the sample size (n = number of mice) for each experiment. Data represent a single (2 year) experiment. Statistical significance was assessed using one-way ANOVA unless otherwise stated in the figure legends. Data are presented as means ± standard error of the mean (SEM) unless otherwise stated in the figure legends with $p < 0.05$ considered statistically significant.